FEDERAL UNIVERSITY OF SAO CARLOS
CENTER OF EXACT SCIENCES AND TECHNOLOGY
GRADUATE PROGRAM IN MATERIALS SCIENCE AND ENGINEERING

ANALYSIS OF TOOL TRAVERSE SPEED IN FRICTION STIR WELDING OF AZ31 MAGNESIUM ALLOY THIN PLATES

Fernanda Rocha Chiuzuli

São Carlos – SP
2021

FEDERAL UNIVERSITY OF SAO CARLOS
CENTER OF EXACT SCIENCES AND TECHNOLOGY
GRADUATE PROGRAM IN MATERIALS SCIENCE AND ENGINEERING

ANALYSIS OF TOOL TRAVERSE SPEED IN FRICTION STIR WELDING OF AZ31 MAGNESIUM ALLOY THIN PLATES

Fernanda Rocha Chiuzuli

Dissertation presented to the Graduate Program in Materials Science and Engineering (PPGCEM) in partial fulfillment of the requirements to obtain the MASTER DEGREE IN MATERIALS SCIENCE AND ENGINEERING

Supervisor: Prof. Dr. Claudio Shyinti Kiminami
Co-supervisor: Prof. Dr. Piter Gargarella
Finance agency: CNPq 130501/2019-0

São Carlos – SP
2021

DEDICATION

To my grandfather João Chiuzuli, who is present through the beautiful memories left.

VITAE

Bachelor of Materials Engineering from the Federal University of Sao Calos (2018)

UNIVERSIDADE FEDERAL DE SÃO CARLOS

Centro de Ciências Exatas e de Tecnologia
Programa de Pós-Graduação em Ciência e Engenharia de Materiais

Folha de Aprovação

Defesa de Dissertação de Mestrado da candidata Fernanda Rocha Chiuzuli, realizada em 25/02/2021.

Comissão Julgadora:

Prof. Dr. Piter Gargarella (UFSCar)

Prof. Dr. Claudemiro Bolfarini (UFSCar)

Prof. Dr. Athos Henrique Plâine (UDESC)

O presente trabalho foi realizado com apoio da Coordenação de Aperfeiçoamento de Pessoal de Nível Superior - Brasil (CAPES) - Código de Financiamento 001.
O Relatório de Defesa assinado pelos membros da Comissão Julgadora encontra-se arquivado junto ao Programa de Pós-Graduação em Ciência e Engenharia de Materiais.

ACKNOWLEDGMENT

I thank my parents Claudia and Valdevino for allowing me to dream. To my siblings Danieli and Vitor for encouragement and inspiration. To my grandmother Amélia for her life teaching. To Luã for the great companionship.

To my friends Débora and Monise for sharing to all my achievements. To Bruna, Giovanna, Janaina, Jéssica and Micheli for the partnership at Edmundsthal, in particular, to Bruna for the partnership in academic writing. To Mariana Zan for the partnership at Bourbon.

To professor Nelson Guedes de Alcântara for the great opportunity at a time of so many uncertainties. To professor Piter Gargarella for the teachings since undergraduation. To professor Claudio Shyinti Kiminami for his disponibility to guide me in these last months. To professors Claudemiro Bolfarini and Guilherme Koga for their contributions to the qualification. To Luciano Bergmann for the experience and technique shared. And to all of them for being references in the research for me.

To all of the Materials Engineering Department at UFSCar (DEMa) for contributing to my academic and, mainly, personal training. To Federal University of Sao Carlos, Graduate Program in Materials Science and Engineering (PPGCEM) for providing an amazing environment for my academic training. To Helmoltz-Zentrum Geesthacht (HZG) for its enriching technical experience.

I am grateful for the finance of this research. This study was financed in part by the Coordenação de Aperfeiçoamento de Pessoal de Nível Superior - Brasil (CAPES) - Finance Code 001. The activities developed in Germany were promoted by Helmoltz-Zentrum Geesthacht - HZG.

ABSTRACT

The automotive industry's great interest in lightweight materials, such as magnesium alloy AZ31, reflects the growing importance of reducing cars' weight. One of the challenges of using such alloys is that their welding using conventional fusion methods does not result in good mechanical properties. The low corrosion resistance typical of these alloys makes it necessary to search for new welding methods, such as solid-state processes as Friction Stir Welding (FSW). However, the literature about AZ31 magnesium alloys welded by FSW revealed the absence of a consensus on the best process parameters for thin plates' welding as plates used in automotive seats. Therefore, this work aims to analyze the best combinations of parameters to weld a 2 mm thick AZ31 magnesium plate by FSW to obtain welds without defects and with good mechanical performance. To meet this objective, AZ31 plates were welded in two configurations (butt - BW and overlap – OW), varying only the tool traverse speed, and their mechanical properties were analyzed by tensile, shear, three-point bending tests, and microhardness, and the microstructure was observed by optical microscopy. About the surface finish, the lowest speeds resulted in flashes formation due to high-temperature development. For BWs, the UTS average increased when the speed increased until 2 m/min, becoming constant for speeds upper to 2m/min. For OWs, shear stress values initially increased due to grain refining, however decreasing with high speeds due to the formation of the large voids. The hardness profiles were not affected a lot by speed, since its increase resulted in grain refinement.

Keywords: AZ31; Magnesium Alloys; Friction Stir Welding; Solid-state welding; Butt Joint Configuration; Overlap Joint Configuration.

RESUMO

ANÁLISE DA VELOCIDADE DE AVANÇO DA FERRAMENTA NA SOLDAGEM POR FRICÇÃO NO ESTADO SÓLIDO DE PLACAS FINAS DA LIGA DE MAGNÉSIO AZ31

O grande interesse da indústria automotiva por materiais leves, como a liga de magnésio AZ31, reflete a crescente importância de reduzir o peso dos carros. Um dos desafios do uso dessas ligas é que a soldagem por métodos convencionais de fusão não resulta em boas propriedades mecânicas. A baixa resistência à corrosão, típica dessas ligas, torna necessária a busca por novos métodos de soldagem, como o processo de soldagem por fricção no estado sólido (FSW). Contudo, a literatura sobre as ligas de magnésio AZ31 soldadas pelo FSW revelou a ausência de consenso sobre os melhores parâmetros de processo para soldagem de chapas finas, tais quais utilizadas em assentos automotivos. Portanto, este trabalho tem como objetivo analisar as melhores combinações de parâmetros para soldar uma placa de magnésio AZ31 de 2 mm de espessura por FSW para obter soldas sem defeitos e com bom desempenho mecânico. Para atender a esse objetivo, as placas AZ31 foram soldadas em duas configurações (topo (BW) e sobreposição (OW)), variando, apenas, a velocidade de deslocamento da ferramenta, e suas propriedades mecânicas foram analisadas por ensaios de tração, cisalhamento, flexão em três pontos e microdureza, a microestrutura foi observada por microscopia óptica. Sobre o acabamento superficial, as menores velocidades resultaram na formação de flashes devido ao desenvolvimento de altas temperaturas. Para BWs, o UTS médio aumentou com o aumento da velocidade até 2 m/min. Para OWs, os valores de tensão de cisalhamento inicialmente aumentaram, devido ao refino de grão, porém diminuíram com altas velocidades devido à formação de grandes vazios. Os perfis de dureza não foram muito afetados pela velocidade, já que seu aumento resultou no refinamento de grão.

Palavras-chave: AZ31; Ligas de Magnésio; Solda por fricção e mistura; Soldagem no estado sólido; Solda topo a topo; Solda com sobreposição.

LIST OF CONTENTS

LIST OF TABLES

LIST OF FIGURES

SYMBOLS AND ABBREVIATIONS

AS	Advancing Side
AZ31	AZ31 magnesium alloy
BT	Bending Test
BW	Butt Weld
DRX	Dynamic Recrystallization
E.C. E	United Nations Economic Commission for Europe
EPA	Environmental Protection Agency
EST	Effective top sheet thickness
FSW	Friction Stir Welding
HAZ	Heat-Affected Zone
HC	Hexagonal Crystal Structure
HZG	Helmoltz-Zentrum Geesthacht
LST	Lap Shear Test
NHTSA	National Highway Traffic Safety Administration
OW	Overlap Weld
RD	Rolling direction
RS	Retreating Side
RSW	Resistance Spot Welding
SZ	Stir Zone
TIG	Tungsten Inert Gas
TMAZ	Thermo-Mechanically Affected Zone
TT	Tensile Test
TWI	The Welding Institute
UTS	Ultimate tensile strength
YS	Yield strength

1 INTRODUCTION

The emission of greenhouse gases has become a significant problem with industrial development, and fossil fuel consumption has increased. The automobile industry is a clear example of an industrial sector that involves a large emission of greenhouse gases during its production process, as well as afterward since it inserts its cars into society, which throughout its use will produce greenhouse gases as a result of the burning of fossil fuels. In this global context, international environmental protection agencies, such as Environmental Protection Agency (EPA) and National Highway Traffic Safety Administration (NHTSA), created regulations that require new cars with less fuel consumption [1].

Thus, a vehicle industry alternative to reduce greenhouse gases emission is reducing vehicles' weight. Furthermore, this weight reduction satisfies environmental and commercial interests since reducing and optimizing the car fuel consumption makes it more competitive [1]. Also, extending the interest in the near future, automobile's weight reduction is adequate for electric vehicles, which have their autonomy directly related to the car weight [2].

Consequently, the ways to achieve weight reduction are changes in design or/and materials. Many automotive companies, such as General Motors (GM), Ford, Volkswagen, and Toyota, have been increasing the use of lightweight materials such as magnesium, looking for a way to replace parts usually produced in steels [3]. Studies have shown the possibility of replacing around 22 structural parts of cars with magnesium [1]. Among the most diverse potentially replaceable parts, car seats have become an option.

By directly interfering with driver safety, car seats require several studies to ensure that the replacement does not lead to loss of properties, such as shock and fatigue resistance. Furthermore, the thin plates prevalence in the seat structures adds another processing requirement that involves the welding process suitable for this new material and, also, for small thickness.

However, the use of magnesium in some structures requires attention to the welding process because one of the major Mg alloys' challenge is the poor weldability, resulting in porosity formation during the conventional fusion welding

processes such as Tungsten Inert Gas (TIG) and Resistance Spot Welding (RSW) [4, 5]. Consequently, the Friction Stir Welding (FSW), a solid-state joining process, is a promising technique in this context, since it enables the magnesium use because this welding process does not involve melting the material, but only the plasticization of it, which avoids the problems of magnesium oxidation [6].

Several studies on FSW of AZ31 were carried out, including studies involving thin plates (2 mm thick). However, the choice of the FSW as a welding method brings with it a diversity of parameters combinations inherent to such process, related to the process (tool traverse speed, tool rotation speed, and tilt angle), tool (diameter, length, and material), and design (butt, overlap joint configuration and others). Literature works show no consensus about which parameters to use when the thickness of the AZ31 plate is fixed at 2 mm [7-11]. For butt welds (BWs) on 2 mm thick plates, the study by Commin et al. [7] finds an optimization window through lower limits for the ratio of tool rotation speed (ω) and the tool traverse speed (v), $\omega 2/v > 4000$ rpm2min/mm, as well as for the tool traverse speed, $v > 0.2$ m/min. For the welds performed with overlap, other studies such as Yang et al. [8], Yuan et al. [9], and Moraes et al. [10] explored AZ31 plates of the same thickness (2 mm) but suggested different values of tool traverse and rotation speeds.

Moreover, some studies, as Ugender et al. [11], converge on the greater importance that tool traverse and rotation speed have in determining the weld properties among the numerous parameters involved in this new welding process. Also, it was seen that considering these two speeds, the traverse speed is the parameter that most differs from one study to another, even when the studies involve plates of the same thickness [7-11]. Therefore, to analyze the best combinations of parameters for welding a 2 mm thick AZ31 plate by FSW, the current work will isolate only one of the two variables mentioned above, tool traverse speed, to then check its influence on the properties of the welds obtained.

2 OBJECTIVE

This project aims to analyze the influence of the tool traverse speed on macro-microstructure and mechanical properties of weld 2 mm thickness plates of AZ31 magnesium alloy by FSW. For this, an extensive literature review was done concerning the FSW of AZ31 plates in butt and overlap configurations. Besides, these plates were welded by FSW and characterized by mechanical tests (tensile, lap shear, bending, and microhardness test) and microstructural analyses (optical microscopy) to establish a correlation between process parameters, structure, and properties.

3 LITERATURE REVIEW

One application of the AZ31 magnesium alloy is in automotive seats aiming at reducing vehicle weight, and the FSW is a welding process to make this application viable. Therefore, this literature review will begin with some aspects involving the automotive seat, from its need for weight reduction to the change in the material used in its structures. In the sequence, the magnesium alloy AZ31, being a potential material for such applications, will be detailed, and, finally, the FSW, the welding process used, will be described.

3.1 Automotive Seat

Among the most diverse parts that make up the cars, the seats have great prominence since it is the structure in which the passenger will be in direct contact for a long time. Considering this, the car seat design must achieve maximum comfort during the passenger's stay, maximum durability compatible with the life of the car, and maximum safety in situations such as sudden braking [12].

The seats are composed of structural frame members and nonstructural frame members, as shown in Figure 3.1. The structure frame members were usually made of steel due to the need to continually support the weight of its structure, as well as the weight of the passenger in various situations of braking, unevenness, and impact. The search for reducing the weight of cars involves reducing the weight of the various components of the seat [12].

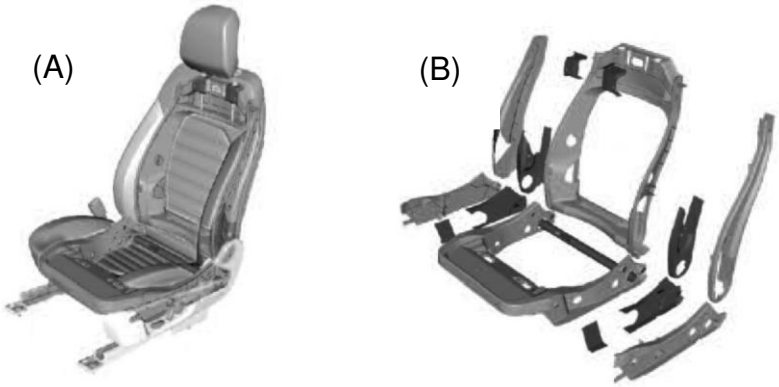

Figure 3.1 - Automotive seat structure. In (A) nonstructural frame members, and in (B) structural frame members *[13]*.

Initially, the most crucial seat property to achieve was a higher mechanical strength to be sure that this structure could resist impacts. The steel came as good material to satisfy immediate mechanical strength requirements. Later, weight reduction emerged as an essential aspect of sports cars. The goal was to improve performance; then, carbon fiber was the most promising material. Currently, as previously exposed, reducing car weight appears as a general requirement for the vehicle industries. Then, not only performance but yet environmental aspects support this necessity. For the actual panorama, magnesium emerges as attractive material due to its lightness and mechanical resistance [13].

In this regard, aiming at a trade-off between safety and strength versus energy- saving, some lighter materials such as aluminum and magnesium have increased importance in the application in some parts of the seat base and backrest component. However, the need to reduce weight through the use of these lightweight materials does not overlap the need to maintain the strength and better energy absorption traditionally achieved by using steel. Therefore, the application of materials such as magnesium, although promising, is still limited to some structures that can be replaced [12].

3.2 Magnesium AZ31

Magnesium has been using in the automotive industry since before the mid-1930s when an engine block in the Volkswagen Beetle was made using magnesium in its composition. From there, many automotive applications have been using magnesium as an alloying element for aluminum, steel, and iron, as a sacrificial anode to protect other metals or as a structural material. The magnesium global demand can be seen in Figure 3.2 which shows a growing demand [14].

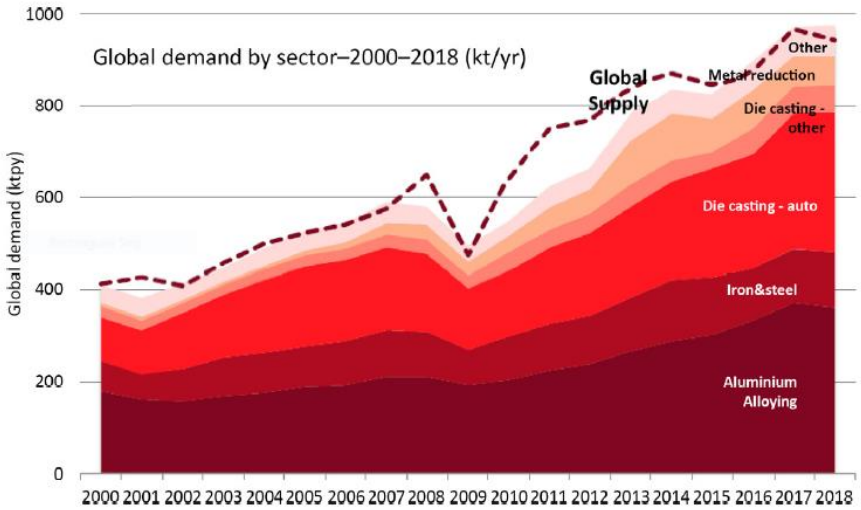

Figure 3.2 - Magnesium global demand by sector since 2000 until 2018 *[14]*.

Considering the use of magnesium as a structural material in cars, different magnesium alloy compositions and processing need to be used. Then, analyzing some alloys of interest, it is possible to verify a range of values for some properties required for car application like ultimate tensile strength (UTS) of 160-365 MPa; yield strength (YS) of 83 - 305 MPa; elongation of 2 - 16 %; shear strength of 125 - 180 MPa and hardness of 49 - 88 HRB [14].

Studies on the implementation of magnesium alloys in this industrial sector show that such alloys have several advantages that justify their growing application. The attractive properties of these alloys allow resulting in an effective reduction of mass, without loss of performance. Among these properties stands out the strength values similar or greater than many traditional automotive aluminum alloys, higher stiffness than many polymeric materials and composites, high fluidity that allows extremely shapes, and excellent damping capability reducing vibration and noises [14].

Despite the large advantages, the high cost of magnesium, the poor weldability and the limited overall design with this material when compared with steel represent some limitations that need to be considered when choosing this material as a substitute. The poor weldability is a consequence of the easy magnesium alloys oxidation forming magnesium oxide with the high melting point, then during the welding process involving material fusion, the reaction of

magnesium with oxygen increases and, consequently, there is greater oxides deposition in the metal pool or forming inclusions in the weld region, which decrease the joint properties. Besides, the reaction of magnesium with nitrogen is also a limitation for fusion welding methods, since the magnesium nitride formed is not stable and compromises the weld properties [14, 15].

Magnesium is the lightest structural metal with an elemental density of 1.74 g/cm3 which is about 60% of the aluminum and less than one-fourth of iron and steel. Besides, the use of magnesium is feasible just when it is alloyed with other elements such as aluminum, zinc, cerium, silver, thorium, yttrium, and zirconia, demonstrating the great variety of elements found in commercial alloys [14, 16].

In this work, the magnesium alloy selected to be used is the AZ31 because it is a magnesium alloy widely used by automotive industries. This alloy has aluminum and zinc as main alloying elements with the following nominal composition by weight: 3 wt.% aluminum and 1 wt.% zinc. The use of other metals provides the proper strength, corrosion resistance, and formability for each alloy. Aluminum is the most used alloy element and its use affect the alloy mechanical properties by intermetallic formation such as Mg17Al12, as shown in the Mg-Al phase diagram (Figure 3.3(A)), which affect the tensile strength, ductility, hardness, and corrosion resistance. The strength improvement can be achieved by intermetallic influence just for processing with the high cooling rate because these intermetallic remain in intragranular position (Figure 3.3(B)) acting as a barrier to slip systems making plastic deformation difficult needing bigger stress application. However, when this alloy is submitted for heat treatment without a high cooling rate, the intermetallic dislocates to the intergranular position (Figure 3.3(C)) acting as a point of concentration stress, and being the intermetallic brittle than the alloy, this second phase decreases the tensile strength [17].

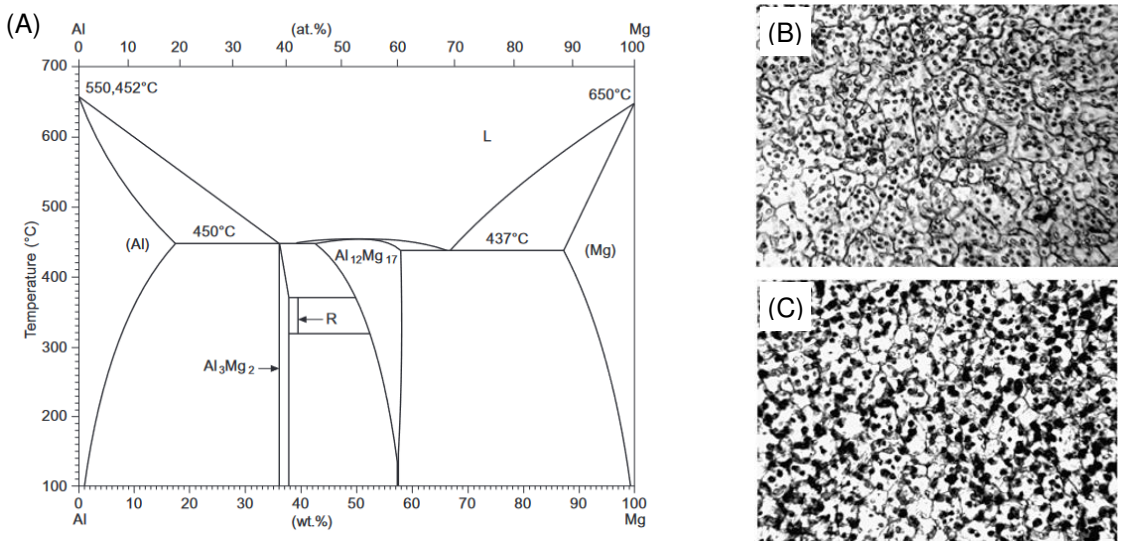

Figure 3.3 - (A) Mg-Al phase diagram, (B) intermetallic in intragranular position, and (C) intermetallic in intergranular position *[17]*.

The zinc as alloying element affect also the alloy mechanical properties. Then, in literature, it is reported that some Zn can change the place of Al in the intermetallic (Mg17Al12) being possible Mg17 (Al, Zn)12 formation, and thus the Zn influence can be similar of the Al, as cited above [17].

The magnesium has a compact hexagonal crystal structure (HC), then the basal slip is the dominant deformation mode in magnesium alloys at room temperatures or below 200° C due to its low critical shear stress. However, at room temperature, the basal slip has only two independent slip systems which result in difficult plastic deformation, and, consequently, low ductility [18].

On the other hand, non-basal slip in prismatic and pyramidal planes occur at room temperature depending on higher stresses, around 50-100 times greater than the stresses for a basal slip. Then an alternative to expanding the AZ31 application is to increase the process temperature to activate other slip systems, and, consequently, to improve the plastic capability that it is essential to increase the possibilities in design [18, 19].

Besides, twins' deformation is also an important mechanism of plastic deformation in magnesium. This deformation mode generally occurs at low temperatures, since, at high temperatures, other mechanisms stand out. In

general, the twins nucleate in the grain's contours or pre-existing twins, and from there, they propagate easily inside the grains [16, 20].

For automotive applications, AZ31 alloy is generally used as a plate. Then the microstructure of these alloys is determining for the temper conditions used such as annealed, O temper, or a partially hard, H-24 temper. The first temper condition determines a microstructure with a homogeneous distribution of grains with clear boundaries, and the second temper, a microstructure highly deformed with no clear grain boundaries. Moreover, both tempered materials presented a typical anisotropy for strength and ductility due to the irregularity of the grain structure and to the texture difference caused by HC structure of the magnesium alloys [14].

3.3 Friction Stir Welding (FSW)

3.3.1 Process Parameters

Since the AZ31 magnesium alloy is an attractive alternative to be used as an automotive seat material and considering its poor weldability due to its easy reaction with oxygen and nitrogen, the AZ31 application needs an alternative welding route. In this way, the FSW is a good option because it is a solid-state joining process and then avoid the magnesium problems related to the fusion process.

The FSW was invented at The Welding Institute (TWI) of the UK in 1991, and this technique involves a non-consumable rotating tool formed by the probe and the shoulder. The main probe functions are to heat, plasticize and mix the material by friction, and the main shoulder functions are to make additional heating by friction and to avoid that the plasticized material go out from the weld zone [6].

Then, the process starts with the rotating probe penetration in the workpiece, heating, and plasticizing the material around it. The combination of rotation and translation movements of the probe makes the plasticized material moved from the front and deposited to the back of the probe, establishing the joint between the plates [6].

Considering the mechanical of this process, two different sides can be determined in the FSW: the advancing side (AS), the side where the tool rotation rate and the tool traverse speed are in the same direction, and the retreating side (RS), where these two parameters are in the different directions. On the AS, the plasticized material is swept for the front of the probe and, on RS, this plasticized material is extruded to the back of the probe. Consequently, due to these mechanical differences between AS and RS, the temperature and the stress developed were higher on RS than AS, as reported by Commin et al. [6, 7].

A challenge for using FSW is to control the various process parameters, which directly interfere with weld quality. The main process parameters (Figure 3.4) involve weld parameters as tool traverse speed (v, mm/min), tool rotation rate (ω, rpm), and axial force (or downward force); tool parameters as geometry (diameter, length, and profile), material and tilt angle; and joint design as butt, overlap, multiple laps, T lap and others [6].

A challenge for using FSW is to control the various process parameters, which directly interfere with weld quality. The main process parameters (Figure 3.4) involve weld parameters as tool traverse speed (v, mm/min), tool rotation rate (ω, rpm), and axial force (or downward force); tool parameters as geometry (diameter, length, and profile), material and tilt angle; and joint design as butt, overlap, multiple laps, T lap and others [6].

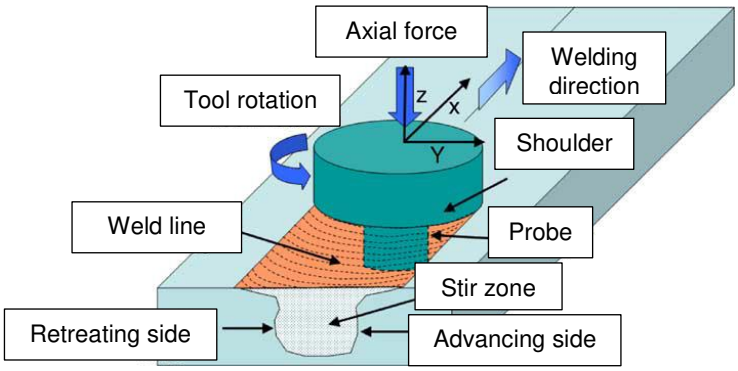

Figure 3.4- Weld parameters and the indication of the two weld sides *[6]*.

About the weld parameters, two important parameters are the tool rotation rate (ω, rpm) in the clockwise and counterclockwise direction and tool traverse

speed (v, mm/min) along the line of the joint. The tool rotation results in mixing and stirring, and the tool translation moves this stirred material from the front to the back of the probe. Then, the tool rotation rate is the parameter that will determine the friction, heating, and plasticization rate, and the tool traverse speed will determine the distribution of these changes generated by the rotation, that is, it will determine the interval in which these thermal and mechanical changes will occur.

In the literature, the combination of these welds parameters by ω^2/V rate was explored by *Commin et al.* [7], and this work shows the process window of $\omega^2/V > 4000$ rpm^2minmm^{-1} for AZ31 2 mm plate welded by FSW. Consequently, these two weld parameters are directly related to the heat input developed in the workpiece. The SZ temperature can be estimated by $\frac{T}{T_m} = K\left(\frac{\omega^2}{V\times 10^4}\right)^{\alpha}$, with T_m the alloy melting point, and α and K constants. Therefore, a higher tool rotation rate generates a higher temperature, and on the other side, a higher tool traverse speed promotes a lower temperature [6, 7].

Moreover, the downward force (or axial force) is also an important weld parameter that determines the insertion depth of the probe. Then, too high axial force generates too shallow insertion, and the shoulder of the tool plunges into the workpiece and produces many flashes, resulting in excessive reduction of the cross-section area of welding. On the other hand, when the axial force is too low, the insertion depth is too deep, and this situation makes the shoulder does not have contact with the workpiece surface and, consequently, it reduces the shoulder capability to move and hold the stirred material.

These three weld parameters interfere in the mechanical properties; however, studies as *Ugender et al*. [11] showed that the tool traverse speed is the most important. A wide range of tool traverse speed has been used, even when considering similar material and thickness. For example, to weld AZ31 2 mm thick plates, values from 0.025 m/min to 2 m/min were used by *Ugender et al.* [11] and *Commin et al.* [7], which shows the wide range of tool traverse speed values found in the literature [7, 11].

Although tool rotational and traverse speed often exert more significant influence, the tool geometry needs to be considered to estimate the material flow and the mechanical properties resulted from some weld processes. Then, determining tool geometry encompasses many aspects as shoulder and probe design (diameter, profile, length, material, and tilt angle), as can be seen in Figure 3.5. It is important to remember that the FSW tool always requires the following characteristics: a shape as simple as possible to reduce the fabrication cost and to promote sufficient stirring effect to produce defect-free welds [11].

The probe is the tool part that makes the first contact with the workpiece, and then it is the main heat generator during the beginning of the FSW. This tool part is responsible too for stirring the plasticized material around itself. The probe parameters include depth, diameter, and profile [6].

The correct probe depth avoids a lack of penetration by the too-short probe. Besides, the diameter and profile of the probe influence the contact area between this tool part and the workpiece, and consequently, the frictional heat generation. Studies of Mishra et al. [6] established the probe influences from the analysis of the ratio between the swept and shoulder volume, which is the ratio between the dynamic and static volume. Then, the higher the ratio, the bigger the volume deformed, and, therefore, the higher the heat generated [6, 21, 22].

Another important tool part is the shoulder, which is the part that helps in the friction and keeps the softened material in the weld zone. The shoulder design variation can be determined from the diameter and profile changes. Then, the shoulder diameter controls how the heat will be generated by friction and how efficient it will be the shoulder to keep the plasticized material in the correct place to avoid defects. Considering the heating, the shoulder diameter is an important parameter because a bigger diameter promotes a higher contact area between the tool and workpiece, and, consequently, higher heat is generated by friction [23, 24].

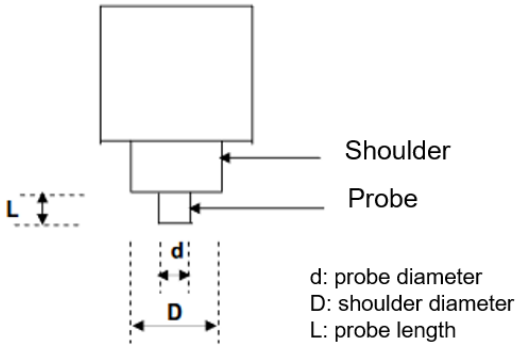

Figure 3.5- Some tool parameters *[23]*.

During the weld by FSW, the material achieves around 70-90% of its melting point, and then the tool needs to be made of a material with sufficient strength in this temperature range, avoiding that the tool twists and breaks. Moreover, the tool material also influences the friction between the tool and the plasticized material. Currently, the tools are made of aluminum alloys and steel, but there are cases where stronger tools are required, and in these cases, a molybdenum alloy is an excellent alternative to be used [25].

Finally, another tool parameter is the tilt angle of the tool to the workpiece. The suitable tilt angle is indispensable to ensure the correct shoulder performance to hold the stirred material in the weld zone and to help the movement of this material from the front to the back of the probe [25].

When planning to use a specific weld process, it needs to be certified if this process can be adapted to this application. In this way, the use of FSW in car seats is made possible due to the wide variety of welding designs possible with this method. Then, for the seat application, a lot of joint designs are necessary, being the major designs the butt and overlap configuration. Figure 3.6 shows the seat regions and the equivalent joint design required for each region.

In the butt joint configuration, one plate is positioned on the side of another with the same thickness, Figure 3.6 (B). In the overlap joint configuration, one plate is positioned over the other, Figure 3.6 (C). For both joint configurations, some care is needed as appropriate cleaning and clamping. The surface clean is preliminary care that needs to be done in the two metal plates to avoid weld

contamination and to facilitate the joint between the plates. The clamping needs to be enough to keep the plates in the correct position and avoid some movements during the welding process. Then, each join configuration requires one specific clamping strategy.

Finally, another tool parameter is the tilt angle of the tool to the workpiece. The suitable tilt angle is indispensable to ensure the correct shoulder performance to hold the stirred material in the weld zone and to help the movement of this material from the front to the back of the probe [25].

When planning to use a specific weld process, it needs to be certified if this process can be adapted to this application. In this way, the use of FSW in car seats is made possible due to the wide variety of welding designs possible with this method. Then, for the seat application, a lot of joint designs are necessary, being the major designs the butt and overlap configuration. Figure 3.6 shows the seat regions and the equivalent joint design required for each region.

In the butt joint configuration, one plate is positioned on the side of another with the same thickness, Figure 3.6 (B). In the overlap joint configuration, one plate is positioned over the other, Figure 3.6 (C). For both joint configurations, some care is needed as appropriate cleaning and clamping. The clean is preliminary care that needs to be done in the two metal plates to avoid weld contamination and to facilitate the joint between the plates. The clamping needs to be enough to keep the plates in the correct position and avoid some movements during the welding process. Then, each join configuration requires one specific clamping strategy.

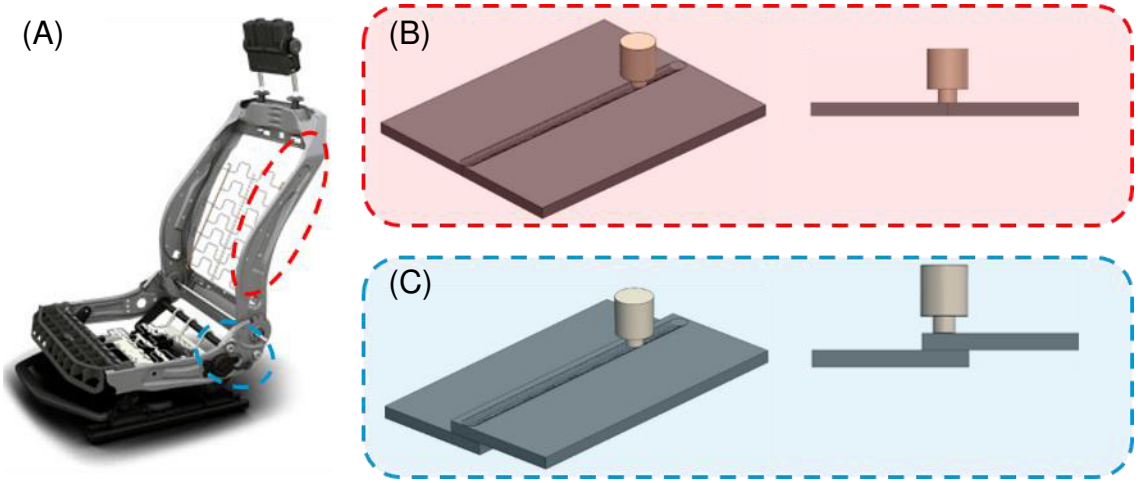

Figure 3.6- Seat regions and the equivalent joint design required for each region. Source: Faurecia.

3.3.2 FSW of Magnesium AZ31

The FSW is an alternative to increase the AZ31 viability and use. Previous studies, as Suhuddin et al. [26], showed high joint efficacy (80% - 100%) of magnesium alloys by FSW; thus the FSW is an efficient welding method to be used for magnesium alloys. As exposed above, all process parameters contribute to the weld's characteristics, which involves macroscopic, microscopic, and mechanical aspects as performance in bending, tensile and lap shear test (LST), and hardness [26].

Macroscopically, the surface of the AZ31 plates welded by FSW presents shoulder friction marks (Figure 3.7 (A)), such as semicircle, which is a typical mark of this welding process. Anormal superficial aspects can be present as flashes, lack of fill, grooves, and others. However, flash formation (Figure 3.7 (B)) is the most common surface defect, and it is formed by plasticized material under the tool shoulder region, which is ejected and extruded on the surface sides of the weld line forming this damage [27].

Normally, the flashes are caused by the excessive heat input that softens excessively the SZ material, or by the low axial force that is insufficient to maintain the plasticized material below the shoulder. Thus, one way to reduce flashes formation is by increasing the tool traverse speed and axial force and decreasing

the tool rotation rate, which would reduce the heat input and increase the plasticized material's containment. According to Abdulaziz [27], the greater the surface texture, the greater the surface stress concentration, and, consequently, the weaker the weld [27, 28].

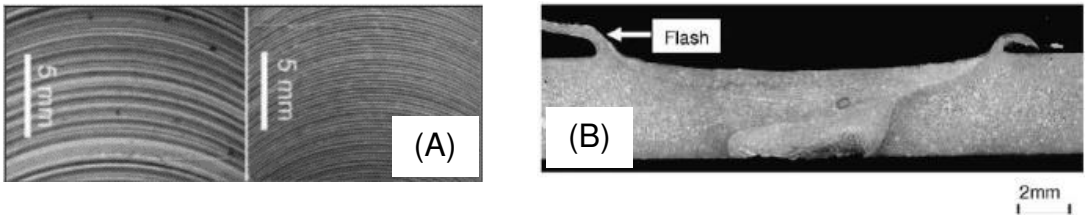

Figure 3.7- (A) Shoulder friction marks, and (B) flashes *[27]*.

Besides, the macroscopical cross-section analyses can detect voids and microcracks which resulted from insufficient heat and improper mixing and pressure. Lack of penetration, when substantially large, also can be detected just by macroscopic analyses, and this defect is caused by a short probe length [27]. Due to the high temperature, enough to plasticize the material, and the complex material movement with intense plastic deformation, the AZ31 welds present a characteristic FSW microstructure with three typical regions (stir zone (SZ), thermo-mechanically affected zone (TMAZ), and heat-affected zone (HAZ)) as indicated in Figure 3.8.

The SZ is the zone that undergoes the highest deformation and increase in temperature because it is the region closer to the probe. Then, the SZ presents fine and equiaxed grains formed during dynamic recrystallization (DRX), with no twins due to the high temperature. According to Mironov et al. [29], the SZ also develops high dislocation density and a {0001} <uwtv> β-fiber texture. The temperature achieved in the FSW is insufficient to the β-phase $Mg_{17}Al_{12}$ particles dissolution; thus, this intermetallic formed in the BM will remain present at SZ after welding [30, 31].

The next region is the TMAZ, which will undergo a lower deformation as well as lower peak temperatures. This region is characterized by the presence of elongated grains caused by the shearing and flow of material around the rotating tools that result in fragmentation and formation of fine equiaxed grains near the

interface between TMAZ and SZ. Next to the TMAZ, there is the HAZ that is the zone influenced only by the thermal cycle, and the microstructure is characterized by the presence of large grains because of grain growth [32, 33].

The microstructure developed in the weld is influenced by many aspects like material, welding parameters, tool geometry, and joint design. Thus, these three typical zones are observed in materials with low recrystallization rates, such as Al alloys. On the other hand, materials with high recrystallization rates, such as austenitic stainless steels and Ti alloys, can develop just two zones being SZ and HAZ. In this second situation, there is no TMAZ because this entire region is recrystallized, having the same SZ microstructure since the recrystallization is easily induced. Besides, the thermal conductivity of each material influences both weld zones and grain sizes. The schematic of Figure 3.8 exemplifies the different weld zones formed during FSW of different materials [32, 33].

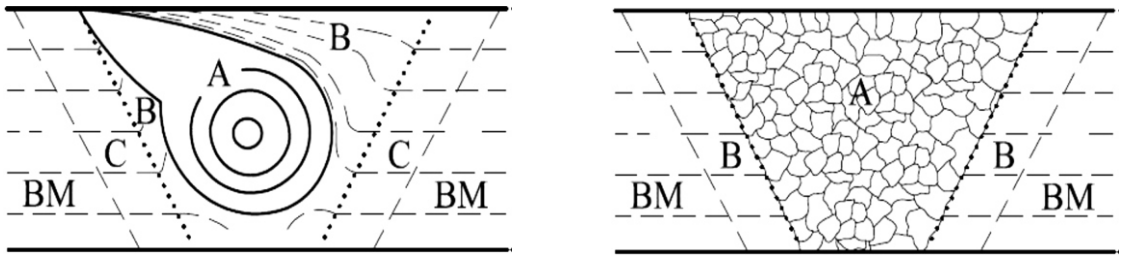

Figure 3.8- The typical zones in FSW: (A) Stir zone – SZ; (B) Thermo-mechanically affected zone – TMAZ; (C) Heat-affected zone – HAZ; and (BM) Base material *[32]*.

The AZ31 welds by FSW have mechanical properties strongly related to the thermo-mechanical input during the tool passing. The three typical zones explained above are not homogenous regions. Pan et al. [34] presented a comparison of numerical model prediction through Lagrangian particle models and experimental observation for different portions of the TMAZ to see the non-homogenous behavior in this zone. On the other hand, Kim et al. [35] simulated the different portions behavior of the SZ for AZ31 welded by FSW, checking the non-homogeneous microstructure of this zone [34, 35].

Furthermore, by microtextural analysis and polycrystalline modeling, Kim et al. [35] concluded, using electron backscatter diffraction (EBSD) analyses, that the FSW process develops a strong fiber texture in the SZ, and this texture varies with the material position with respect to probe rotation. Suhuddin et al. [26] studied the grain structure evolution during the FSW of AZ31, and the results showed that the grain structure undergoes a complex process. Considering the material far ahead of the tool, the material undergoes $\{10\bar{1}2\}$ twinning. Besides, the material closer to the tool has the microstructure determined by the geometric effects of the strain and by the limited discontinuous recrystallization. The material directly near the tool has the grain structure closely linked with the development of texture [26, 35].

The strong texture in the transition region between SZ/TMAZ resulted from the high anisotropy of the magnesium. This microstructure developed in the SZ/TMAZ region is a softening point when submitted to perpendicular tensile because promotes basal slip activation and twinning extension [36].

As described before, for automotive applications, basically butt and overlap FSW designs need to be explored. Thus, each design has important peculiarities in its typical microstructure. In the butt joint configuration, the joining of two plates parallel aligned makes the weld roots a point of constant attention, as can be seen in Figure 3.9. As previously mentioned, if the lack of root filling is large, this defect can be visually detected. However, for small root defects, the bending test (BT) is essential since this test will apply a force across the weld line surface, and consequently, will result in longitudinal stress of the weld root. The analysis of the region where the fracture starts allows inferring if there is a lack of root filling.

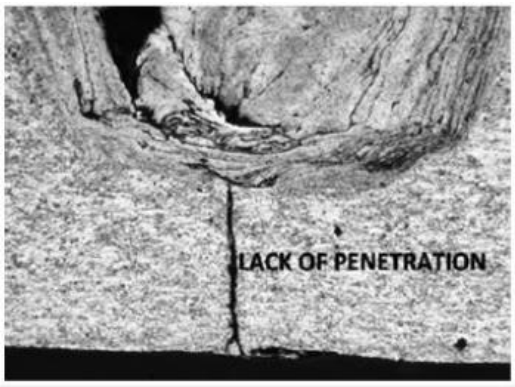

Figure 3.9- Lack of root filling by lack of penetration *[27]*.

For overlap joint configuration, the joint of two overlapping plates commonly results in two discontinuities: the hooking and the cold lap, as shown in Figure 3.10. The hooking is formed due to the downward motion of the material in front of the tool, and after it is deposited in the wake of the pin, and the cold lap is resulted from a complex set of material movement. According to literature, generally hooking is formed on the AS, and the cold lap on RS. The hooking can be with its curvature to up (Figure 3.10 (A)) or down (Figure 3.10 (B)), being the hooking with down curvature related with voids and defects formation in the SZ [9].

According to Abdulaziz [27], the hooking and cold lap formation is highly influenced by the tool rotation ratio, and little influenced by tool traverse speed because they are more related to the material flow generated for the probe rotation. Also, the formation of these discontinuities results in stress concentration and decreases the effective top sheet thickness (EST), which reduces the crack propagation way until the fracture [27].

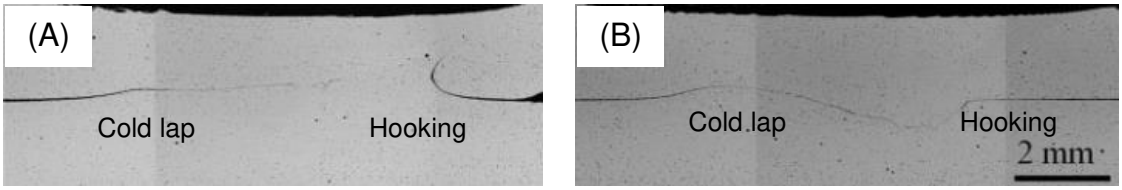

Figure 3.10- Descontinuites in overlpap joints. In (A) hooking with upper curvature, and (B) hooking with down curvature *[9]*.

Studies of AZ31 butt joints [7, 11, 29, 37] achieved considerable results that contribute to and direct the present work. These previous studies have been done to explore the big diversity of the BW aspects. Commin et al. [7] explored the influence of the processing parameters in the FSW of AZ31 for rolled plates. This work used a rolled plate of 2 mm of thickness and four welding conditions: 1000 rpm/200 mm/min, 1300 rpm/300 mm/min, 1400 rpm/700 mm/min, and 600 rpm/2000 mm/min. The tool parameters used were concave shoulder with diameters of 10 mm and 13 mm and threaded probe with a diameter of 5 mm. Finally, the process window achieved for AZ31 plate with 2 mm of thickness was $v > 200$ mm/min and $\omega^2/v > 4000$ rpm^{2}min/mm [7].

Mironov et al. [29] studied the microstructural evolution during FSW of AZ31. This study used the extruded plate with 4 mm of thickness, a range of rotational speeds of 300 to 3000 rpm, and a constant traverse speed of 200 mm/min. The tool parameters were steel tool, concave shoulder, shoulder diameter of 15 mm, threaded cylindrical probe, and probe length of 3.7 mm [29]. Ugender et al. [11] developed a study about the influence of the tool traverse and rotation speed, and tool design in mechanical properties. In this work was used a rolled sheet of 5 mm of thickness, the welding parameters used were rotational speed of 900, 1120, and 1400 rpm; and traverse speed of 25, 40, and 75 mm/min. The tool parameters were probe diameter of 6 mm; probe length of 4.8 mm; shoulder diameter of 18 mm; tilt angle of 2°, and probe designs of taper threaded, taper cylindrical, and straight cylindrical. Combining these welding and tool parameters, nine different welds were compared [11].

Finally, the analysis of defect formation was explored for Gulati et al. [37] that analyzed welds made by a hot rolled plate with 6 mm of thickness. The welding parameters were rotational speed of 1500 rpm and 1800 rpm, traverse speed of 100 mm/min, and 120 mm/min. The tool material was steel with two different shoulder profile, cylindrical and conical, shoulder diameter of 18 mm, probe length of 5.45 mm, and tilt angle of 3°. The work concluded that the cylindrical threaded probe reduces the defect formation on the welds [37].

The overlap joint configuration for AZ31 is an FSW configuration that there are also many studies about. Then, these studies are important to direct the weld

and tool parameters in a specific application. In addition to the variables presented for the butt joint configuration, in the overlap joint configuration, two important additional variables are the side of the joint (AS or RS) that is positioned in the weld line side and the overlap dimension.

The previous studies for the overlap joint configuration explored the influence of the tool geometry and process condition. Yang et al. [8], for example, welded AZ31 plate with 2 mm of thickness, and the weld parameters were tool rotational speed of 1500, 2000, 2500 rpm, and tool traverse speed of 100, 200, 350, and 500 mm/min and overlap of 40 mm. The tool parameters were concave shoulder, shoulder diameters of 12 and 14 mm, cylindrical threaded probe, probe diameter of 4, and 5 mm. The two positions were presented in this study. Then, both AS and RS were positioned on the weld line side [8].

Another work [9] explored the effect of the top sheet behavior when submitted to different probes and shoulders. Then, three tools were used to compare the hook and cold lap formation and, finally, the lap shear performance for each case. Yuan et al. [9] used the AZ31 plate with 2 mm of thickness, and the three tool designs were (1) convex scroll shoulder with 13 mm diameter and triflate threaded probe with 4.7 mm of diameter and 6 mm of length; (2) concave shoulder with the same diameter and probe design; (3) the same second tool with the shoulder diameter of 12 mm [9].

Finally, other important variables of the FSW in an overlap configuration were explored for Moraes et al. [10] and correlated with mechanical behavior. The overlap orientation was analyzed by fatigue performance and LST. The AZ31 plates with 2 mm of thickness were welded in two different configurations changing the side (AS and RS) that was joining in the weld line side. This study showed that the different weld positions influence the formation of hooking, cold lap, and faying surface, and these results in different mechanical performance [10].

Mironov et al. [29] studied the microstructural evolution during FSW of AZ31. This study used the extruded plate with 4 mm of thickness, a range of rotational speeds of 300 to 3000 rpm, and a constant traverse speed of 200 mm/min. The tool parameters were steel tool, concave shoulder, shoulder diameter of 15 mm, threaded cylindrical probe, and probe length of 3.7 mm [29].

Ugender et al. [11] developed a study about the influence of the tool traverse and rotation speed, and tool design in mechanical properties. In this work was used a rolled sheet of 5 mm of thickness, the welding parameters used were rotational speed of 900, 1120, and 1400 rpm; and traverse speed of 25, 40, and 75 mm/min. The tool parameters were probe diameter of 6 mm; probe length of 4.8 mm; shoulder diameter of 18 mm; tilt angle of 2°, and probe designs of taper threaded, taper cylindrical, and straight cylindrical. Combining these welding and tool parameters, nine different welds were compared [11].

Finally, the analysis of defect formation was explored for *Gulati et al.* [37] that analyzed welds made by a hot rolled plate with 6 mm of thickness. The welding parameters were rotational speed of 1500 rpm and 1800 rpm, traverse speed of 100 mm/min, and 120 mm/min. The tool material was steel with two different shoulder profile, cylindrical and conical, shoulder diameter of 18 mm, probe length of 5.45 mm, and tilt angle of 3°. The work concluded that the cylindrical threaded probe reduces the defect formation on the welds [37].

The overlap joint configuration for AZ31 is an FSW configuration that there are also many studies about. Then, these studies are important to direct the weld and tool parameters in a specific application. In addition to the variables presented for the butt joint configuration, in the overlap joint configuration, two important additional variables are the side of the joint (AS or RS) that is positioned in the weld line side and the overlap dimension.

The previous studies for the overlap joint configuration explored the influence of the tool geometry and process condition. *Yang et al.* [8], for example, welded AZ31 plate with 2 mm of thickness, and the weld parameters were tool rotational speed of 1500, 2000, 2500 rpm, and tool traverse speed of 100, 200, 350, and 500 mm/min and overlap of 40 mm. The tool parameters were concave shoulder, shoulder diameters of 12 and 14 mm, cylindrical threaded probe, probe

diameter of 4, and 5 mm. The two positions were presented in this study. Then, both AS and RS were positioned on the weld line side [8].

Another work [9] explored the effect of the top sheet behavior when submitted to different probes and shoulders. Then, three tools were used to compare the hook and cold lap formation and, finally, the lap shear performance for each case. *Yuan et al.* [9] used the AZ31 plate with 2 mm of thickness, and the three tool designs were (1) convex scroll shoulder with 13 mm diameter and triflate threaded probe with 4.7 mm of diameter and 6 mm of length; (2) concave shoulder with the same diameter and probe design; (3) the same second tool with the shoulder diameter of 12 mm [9].

Finally, other important variables of the FSW in an overlap configuration were explored for *Moraes et al.* [10] and correlated with mechanical behavior. The overlap orientation was analyzed by fatigue performance and LST. The AZ31 plates with 2 mm of thickness were welded in two different configurations changing the side (AS and RS) that was joining in the weld line side. This study showed that the different weld positions influence the formation of hooking, cold lap, and faying surface, and these results in different mechanical performance [10].

4 JUSTIFICATION

An extensive literature review on the use of FSW for AZ31 magnesium plates has confirmed the real potential of this welding method as an enabler for applying the AZ31 in automotive seats. Besides, these literature studies showed no consensus on which variables should be used when aiming to weld AZ31 plates with a thickness of 2 mm. Moreover, considering the strong influence of the tool traverse speed on welding properties and its wide range of values used during FSW of 2 mm plates, a systematic study of the effect of this parameter still needs to be done. Consequently, this work aims to investigate the influence of the tool traverse speed on macro-microstructure and mechanical properties of FSW of 2 mm thick AZ31 plates.

5 MATERIALS AND METHODS

In this section will be detailed the materials and methods used. In order to show the procedures used, the diagram below shows the flowchart of the activities performed.

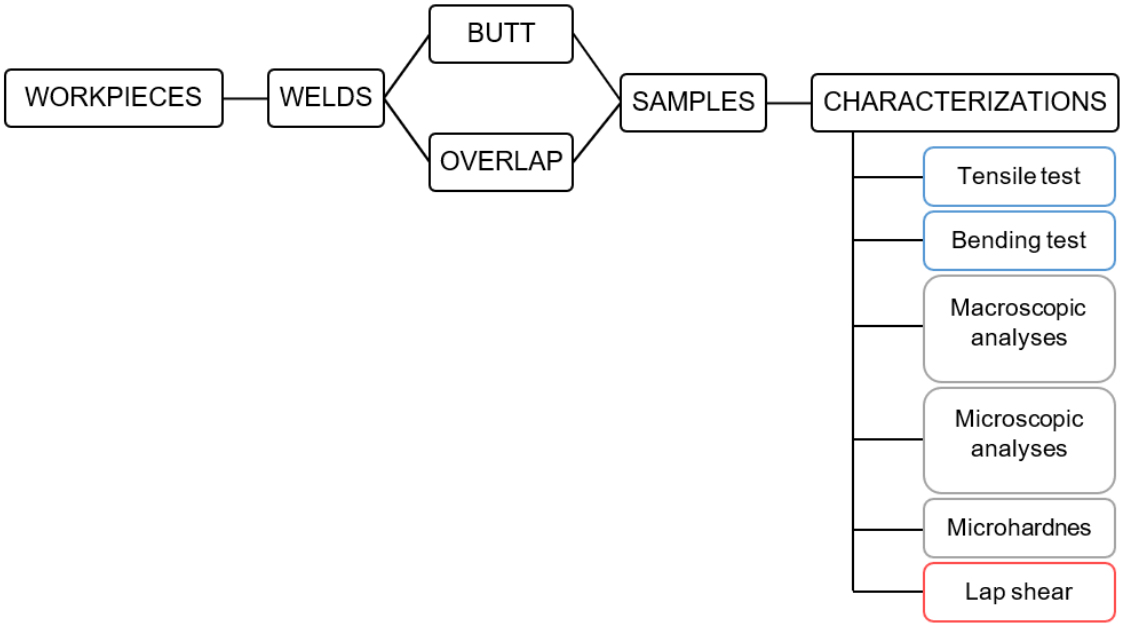

Figure 5.1- Flowchart of the activities sequence. BW characterizations (blue squares), BW and OW characterizations (grey squares), OW characterization (red square).

5.1 Preparation of the Workpieces

The material used in this work was rolled AZ31 magnesium alloy, with nominal chemical composition listed in Table 5.1. The plate dimensions were 475 mm long, 140 mm wide, and 2 mm thick. The workpieces were brushed with sandpaper (#320) and cleaned with acetone minutes before each welding process to remove oxides and other contaminants.

Table 5.1- Chemical composition limits of AZ31 magnesium alloy.

	Al	Zn	Mn	Si	Cu	Ca	Fe	Ni	Mg
Weight (%)	2.5 – 3.5	0.7 – 1.3	0.2 min	0.05 max	0.05 max	0.04 max	0.005 max	0.005 max	Bal.

5.2 Clamping and Welding

The welds were produced at Helmoltz-Zentrum Geesthacht, Germany (HZG), and were obtained perpendicular to the rolling direction (RD) using Portal Anlage weld machine (Figure 5.2 (A)), and, before each welding procedure, a clamping method was studied to avoid inadequate distortions and movements during the process.

The tools were composed of a plan and scrolled shoulder with a diameter of 13 mm, and a triflate and threaded conical probe with a diameter of 5 mm and a length of 1.8 mm and 2.5 mm in the BW and OW, respectively. These tool parameters can be seen in Figure 5.2 (B) and (C).

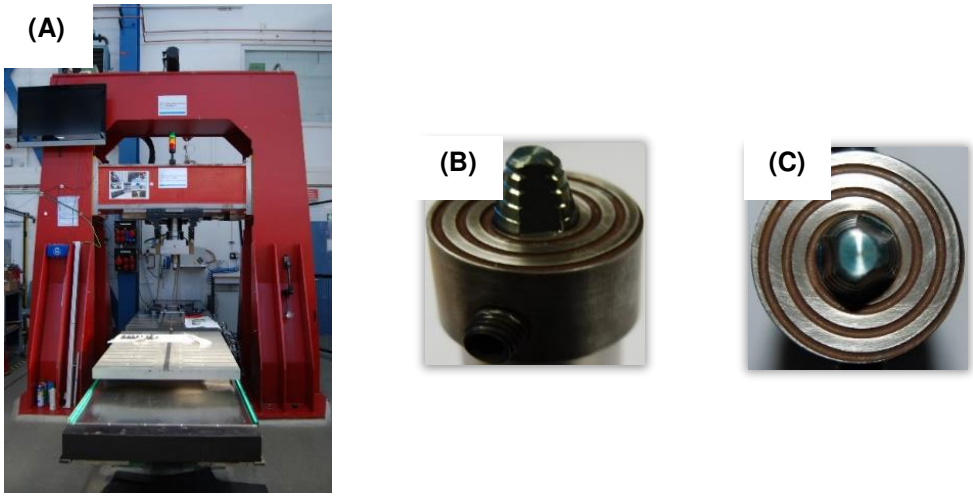

Figure 5.1- (A) Portal Anlage weld machine, (B) picture of the probe, and (C) of the shoulder.

5.2.1 Butt Joint Configuration

The BWs (Figure 5.3) were position-controlled, being the axial force variable to keep the set position. The process consisted of a constant rotational

speed of 2000 rpm, and a tilt angle of 0.5 º, varying the traverse speed from 0.5 m/min until 3.0 m/min, as shown in Table 5.2.

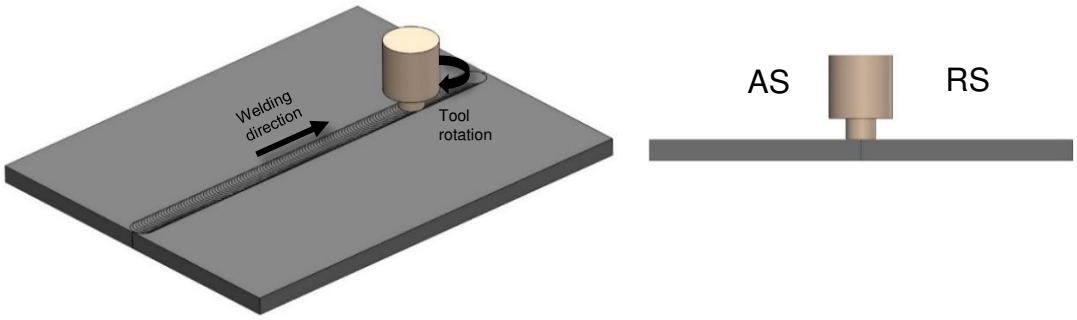

Figure 5.3 - Weld in a butt joint configuration.

Table 5.2: Parameters of welds performed in a butt joint configuration.

Weld	Speed (m/min)	Rotation (rpm)
$BW_{0.5}$	0.5	2000
$BW_{1.0}$	1.0	2000
$BW_{1.5}$	1.5	2000
$BW_{2.0}$	2.0	2000
$BW_{2.5}$	2.5	2000
$BW_{3.0}$	3.0	2000

5.2.2 Overlap Joint Configuration

The OWs (Figure 5.4) were position-controlled and performed with an overlap of 40 mm and in two different configurations, configuration A and B. In configuration A (Figure 5.4 (A)), the AS was positioned in the joint line, and in configuration B (Figure 5.4 (B)), the RS was positioned in the joint line. The process parameters consisted of a constant rotational speed of 2000 rpm, and a tilt angle of 0.5 º, varying the traverse speed from 1.0 m/min until 4.0 m/min, as shown in Table 5.3.

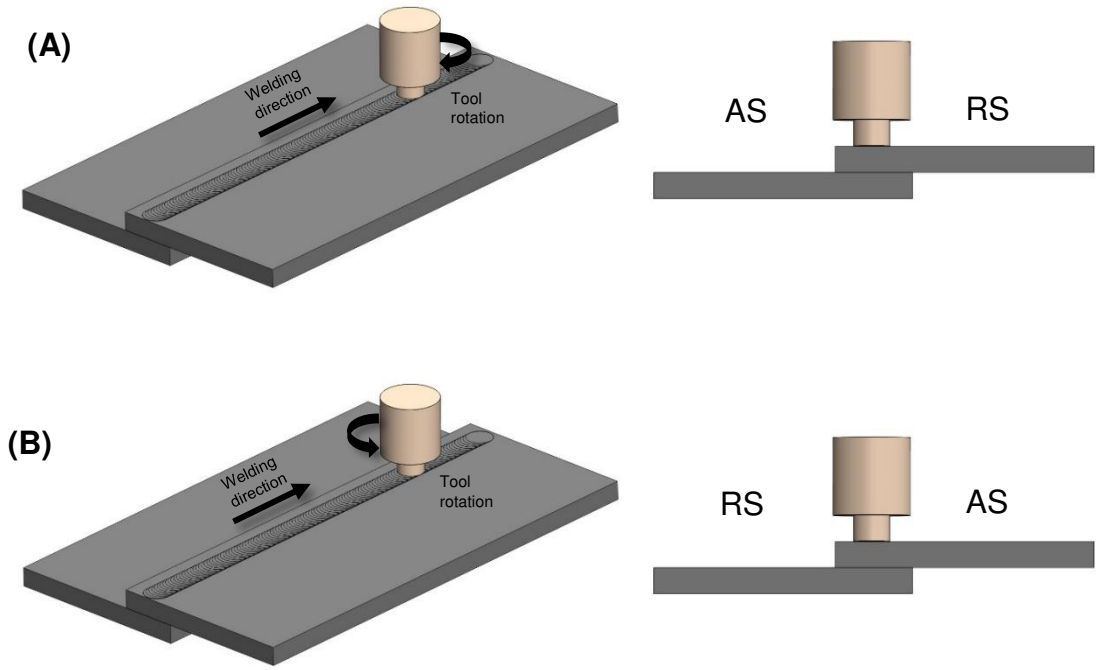

Figure 5.4- The two configurations used to weld the overlap joints: (A) Configuration A: AS in the joint line, and (B) configuration B: RS in the joint line

Table 5.3: Parameters of welds performed in an overlap joint configuration.

Weld	Speed (m/min)	Rotation (rpm)
Configuration A		
OW_{A1}	1.0	2000
OW_{A2}	2.0	2000
OW_{A3}	3.0	2000
OW_{A4}	4.0	2000
Configuration B		
OW_{B1}	1.0	2000
OW_{B2}	2.0	2000
OW_{B3}	3.0	2000
OW_{B4}	4.0	2000

5.3 Cutting and Preparation of Samples

The sample preparation was made at Helmoltz-Zentrum Geesthacht, Germany (HZG). Samples of the BWs were sectioned perpendicularly to the welding direction. For micro and macroscopic analyses, the samples had 40 mm in length and 10 mm in width. For the tensile test (TT), three samples were performed, according to DIN 50125 standard, with 190 mm in length, 24 mm in width, 2 mm in thickness and 25 mm of radius. For the BT, two samples were performed, according to DIN EN ISO 5173 and ASTM E290-09 standards, with 280 mm in length, 20 mm in width and 2 mm in thickness.

Samples were prepared from the OWs in the same way. For micro and macroscopic analyzes, the samples presented the same BW dimensions. For the LST, three samples were performed with 190 mm in length and 25 mm in width. Figure 5.5 shows how the samples were cut in each weld type.

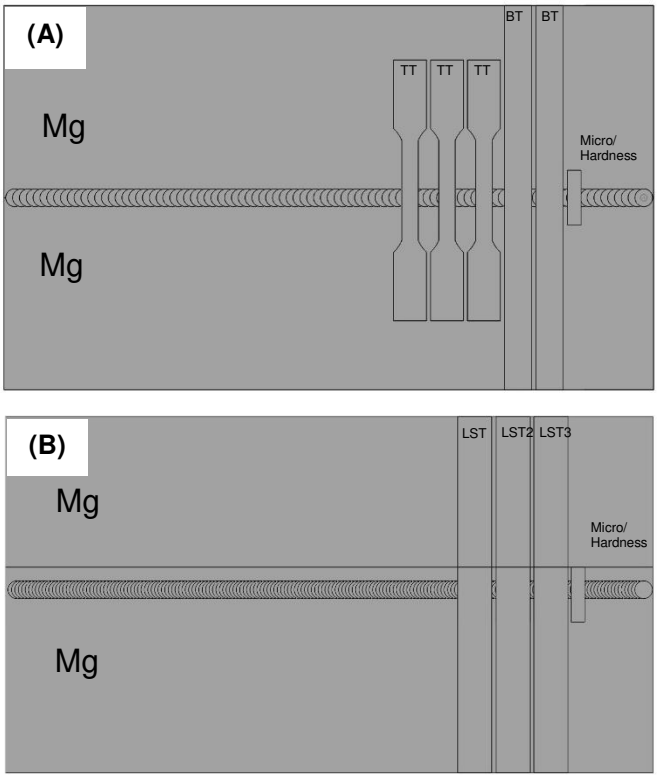

Figure 5.5 - Schematic drawing of the location of the sample in the welds of the (A) butt, and (B) overlap configuration.

5.4 Characterization

5.4.1 Visual Inspection

The visual aspect of the welds was analyzed to check the presence of flashes or superficial damages as lack-of-fill. Then, photographs of the weld's regions were taken to compare their finishing according to each weld parameter.

5.4.2 Macroscopic Analyses

The macroscopic analyses were made, at Helmoltz-Zentrum Geesthacht, Germany (HZG), using Leica SM IRM® optical microscope. The samples were embedded in Demotec-20®, and after cured under pressure. The macroscopic analyses were made in non-etched and in etched samples. The samples were etched during 5 seconds using the solution with 2-3 g of picric acid, 140 mL of ethanol, 30 mL of distilled water and 6.5 to 7 mL of acetic acid. This analysis was done to check the quality of the cross-sectional surface of the weld as well as the occurrence of thickness reduction and/or macroscopic defects in the weld region.

5.4.3 Microscopic Analyses

Microscopic analyses were made to check the grain size and form in each weld zones. Besides, these analyses were made to check the microscopic trend in the transition region between the zones and the presence of microscopic defects.

These analyses were made, at Helmoltz-Zentrum Geesthacht, Germany (HZG), using Leica SM IRM® optical microscope to identify the different welding regions as SZ, thermo-mechanical affected zone (TMAZ), HAZ, and base material (BM). This analysis was done only on the etched samples, being prepared as detailed in the previous item 5.4.2.

5.4.4 Bending Test

To check the integrity of the BWs roots, BTs were made at Helmoltz-Zentrum Geesthacht, Germany (HZG). Then, during the test, it was analyzed if

the fracture started at the weld root, which would suggest a lack of filling and/or root defect.

The parameters used in the BT were based on DIN EN ISO 5173 and ASTM E290-09 standards. According to these standards, the plunger radius is 4 mm (rp = 4 mm), the die radius is 13 mm (R = 13 mm), and the distance between rollers is 14 mm (l = (14 ± 1) mm). Also, the face that undergoes tension should have rounded edges with a radius of 0.4 mm (r = 0.4 mm). The bending test machine used was HIDROALFA, with 200 tons of maximum power and 400 bars of maximum pressure. Figure 5.6 shows a BT machine and an illustrative figure of how the tests were performed and how the angle was measured after the tests.

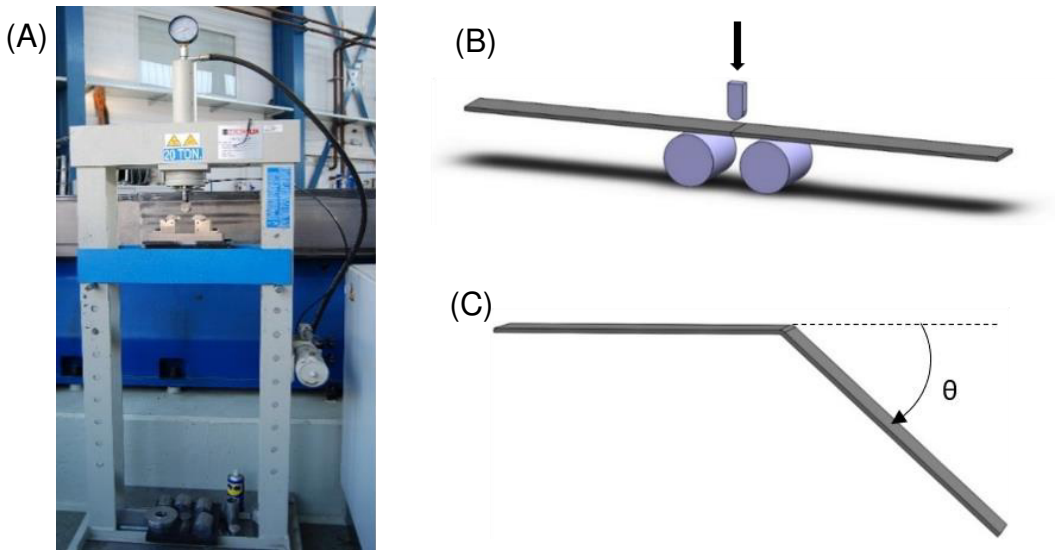

Figure 5.6 – (A) Bending test machine, (B) illustrative image of the BT, and (C) illustrative image of the BT samples with the angle formed after the test.

5.4.5 Tensile and Lap Shear Tests

In order to compare the mechanical performance of each weld produced, the tensile and LSTs were made. The welds were tested, at room temperature, using a screw-driven Zwick/Roell® testing machine with a load capacity of 200 kN. For both tests, the gap between the clamps was 160 mm, and the crosshead speed was 1 mm/min. Figure 5.7 shows the tensile and lap shear samples and the machine used in these tests.

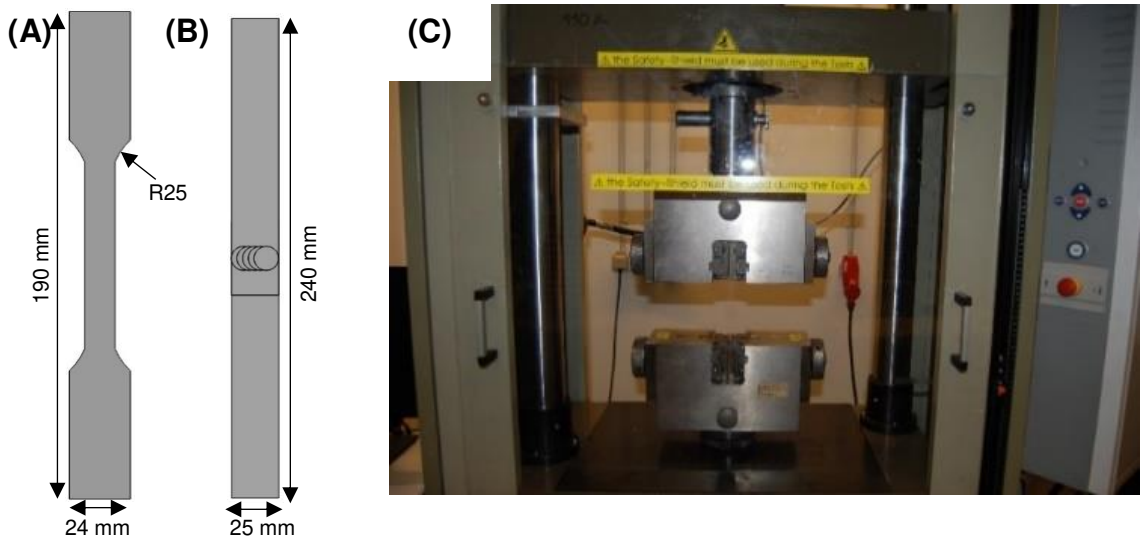

Figure 5.7 – (A) Tensile test sample, (B) lap shear sample, and (C) tensile test machine.

5.4.6 Microhardness

In order to infer the mechanical properties of the different weld regions, microhardness was made. The etched samples used in the microscopic analyses were prepared again and the hardness was made in these non-etched samples. Then, Vickers hardness was carried out horizontally along the cross-section of the welds using the Struers DuraScan® hardness machine. The parameters used were a load of 100 g for 10 seconds with a distance of 0.25 mm between each measurement. Figure 5.8 shows the cross-section measurements for BW (Figure 5.8 (A)) and OW (Figure 5.8 (B)) samples.

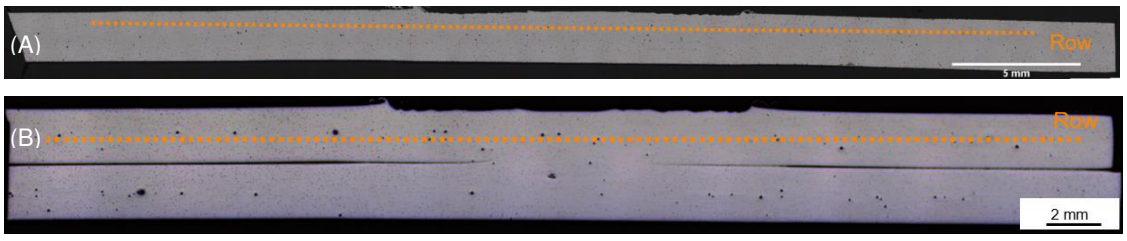

Figure 5.8 - Hardness measurements in (A) BW and in (B) OW.

6 RESULTS AND DISCUSSIONS

6.1 Butt Joint Configuration

6.1.1 Macrostructural Characterization

The superficial The superficial analysis allows checking that the welds in a butt joint configuration presented a good surface finishing, without superficial lack of fill. Apparently, the biggest difference between the welds was the flashes presence in the $BW_{0.5}$ (Figure 6.1 (A)) and $BW_{1.0}$ (Figure 6.1 (B)) in contrast with the clean surface of the other welds. In the FSW, the temperature developed is a combination of tool traverse and rotation speed as discussed by Commin et al. [7]. Since the rotation speed was constant between the welds, the traverse speed was the main determinant for the heat input and, consequently, for the temperature developed. In this way, the higher temperature developed by lower tool traverse speed favors the get out of plasticized material to the shoulder side forming the flashes. This surface difference can be seen in Figure 6.1 that shows the visual inspection for the six welds.

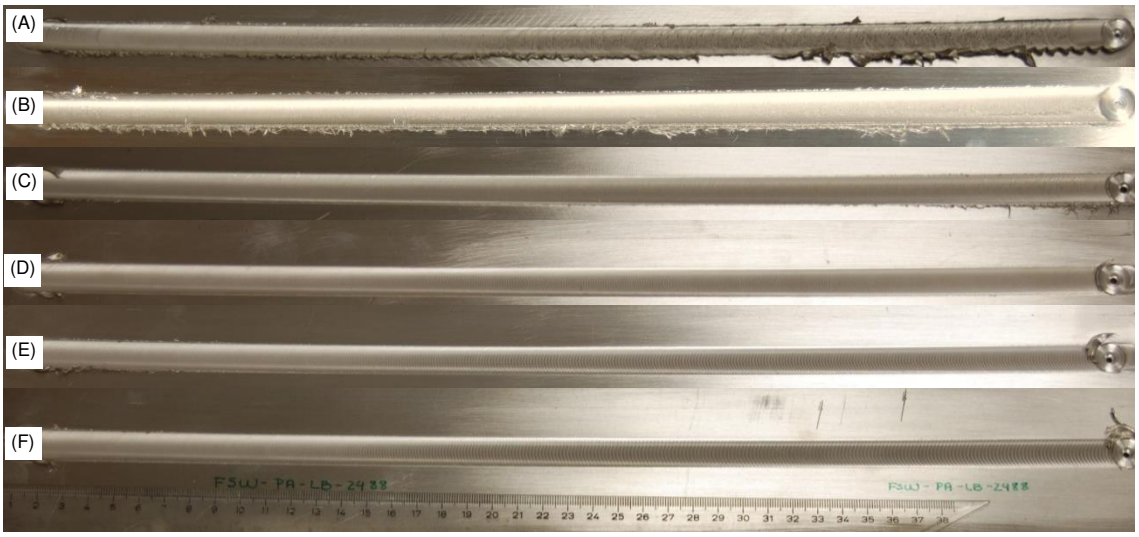

Figure 6.1- Visual inspection of the BWs. (A) $BW_{0.5}$, (B) $BW_{1.0}$, (C) $BW_{1.5}$, (D) $BW_{2.0}$, (E) $BW_{2.5}$, and (F) $BW_{3.0}$.

The cross-sectional surface of the welds was macro and microscopically analyzed. The macrographs of the six welds (Figure 6.2 (A) - (F)) do not show macroscopic defects, but they allow to check flashes at SZ-side (Figure 6.2 (G)) and thickness reduction at SZ (Figure 6.2 (H)). As exposed above, the flashes formed in $BW_{0.5}$ and $BW_{1.0}$ are resulted from the movement of material from the SZ, under the shoulder, to weld surface. Then, this plasticized material moviment results in superficial flashes and thickness reduction..

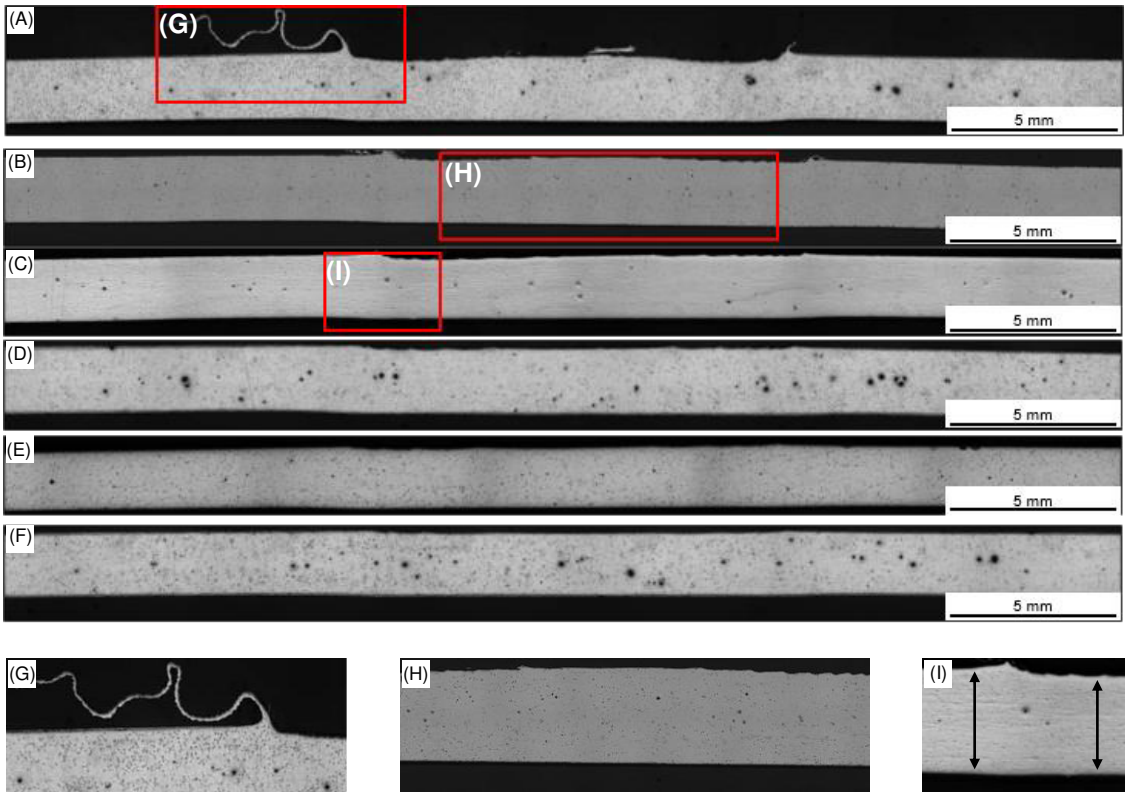

Figure 6.2- Cross sectional analysis (A) $BW_{0.5}$, (B) $BW_{1.0}$, (C) $BW_{1.5}$, (D) $BW_{2.0}$, (E) $BW_{2.5}$, and (F) $BW_{3.0}$, (G) flashes in $BW_{0.5}$ surface, (H) thickness reduction in $BW_{1.0}$, and (I) thickness reduction in $BW_{1.5}$.

6.1.2 Microstructural Characterization

Three typical Three typical weld zones and the transition regions between these zones were checked by microscopic analyses. First of all, the BM (Figure 6.3 (E)) analyses allow seeing that the as-received plate presented equiaxed grains with few lenticular twins, and β-phase $Mg_{17}Al_{12}$ particles undissolved due to the insufficient heating generation during the rolling process,

as observed in Figure 6.3 (B) and reported in some studies [30, 31]. From the weld line to the BM, the first zone observed was the SZ (Figure 6.3 (B)), which is the zone with the highest deformation and temperature development being the region closer to the tool. This region is formed with material that is in direct contact with the tool and with material in indirect contact, which suffers the severe influence of the tool friction. The combination of frictional heating, intense plastic deformation, and viscous dissipation results in one region with fine and equiaxed grains formed by DRX with no presence of twins due to the high temperature, as shown in Figure 6.3 (B). However, the SZ peak temperature is not enough to dissolve the β-phase $Mg_{17}Al_{12}$ particles, then these particles are also present as detailed in Figure 19(B), in the same way as in the BM (Figure 6.3 (E)) [30, 31]. Additionally, the SZ characterizes for high dislocation density and for development of {0001} <uwtv> β-fiber texture, as reported by Mironov et al. [29].

The second zone is the TMAZ (Figure 6.3 (C)). This region is composed of a material that suffers mechanical and thermal indirect action. Then, the microstructure developed in this zone resulted from discontinuous recrystallization or nucleation and grown of grains. Also, no twins are identified since this region's high temperature favors slip system activation as a preferential plastic deformation mode to the detriment of twinning modes. Finally, between TMAZ and BM there is the HAZ (Figure 6.3 (D)), region where just the thermal cycle acts, defining its microstructure with the similar crystallographic orientation to the BM, but with grain grown and extensive $\{10\bar{1}2\}$ twinning as shown in Figure 6.3 (D) [29].

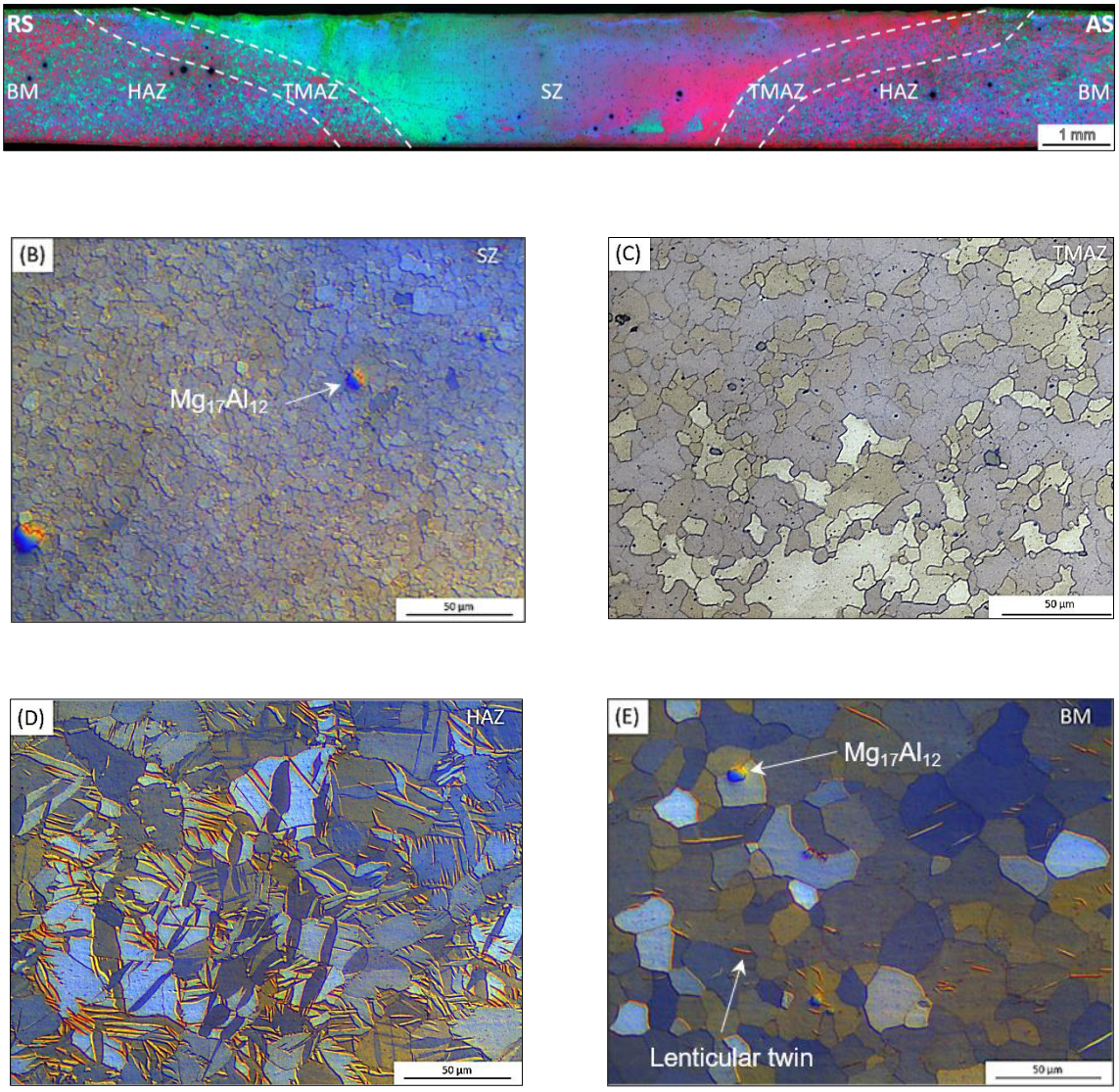

Figure 6.3- Typical FSW areas being (B) SZ, (C) TMAZ, (D) HAZ, and (E) BM.

Another important microstructural aspect is the transition regions between the zones since there is a characteristic microstructure in each zone as detailed above and this discontinuous interface could be a stress concentration point. As discussed above, the SZ/TMAZ region is the more abrupt transition region because there is a drastic difference in grain orientation and twinning activation. The TMAZ/HAZ region characterizes the transition of random high angle boundaries to low angle twin boundaries, and the HAZ/BM does not present significative texture discontinuity but grain size variation. These transitions can be seen in Figure 6.4..

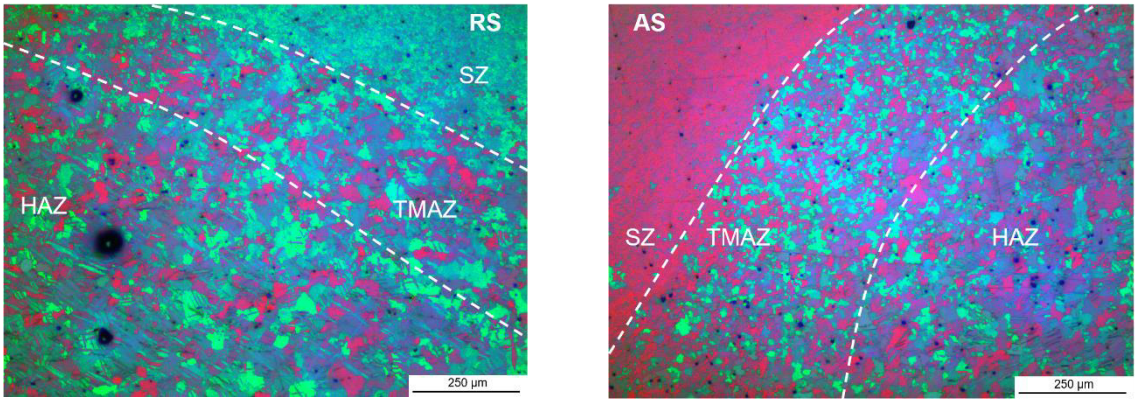

Figure 6.4- Transition regions of FSW samples.

6.1.3 Bending Test

Since the length of the probe is smaller than the plate thickness, the root joint is one critical region because it results from indirect heat transference and plastic deformation caused for the friction between the plates and the tool. The root behavior of the welds was analyzed by BT, which concentrates stress at the root to the qualitative measurement of defects in this region.

First of all, it was found that no weld started to fracture at the root, which suggests having no lack of fill or voids in this region. However, all of them showed fracture started in the transition region between SZ and TMAZ. This generalized fracture behavior is because the FSW usually develops strong local texture in this region, causing a poor mechanical property during the traverse tensile test [38]. According to Liu et al. [38], the SZ/TMAZ transition region does not present a significative grain size difference, but it presents drastically different grain orientations. This clear transition is then characterized by a sudden texture variation that impacts the crack initiation and propagation during the BT.

The twinning is also an important deformation mechanism for magnesium alloys at room temperature being, the twinning activity, highly dependent on the material texture. Then, the expressive texture difference between the SZ and TMAZ results in different twinning activity, contributing to stress concentration and fracture initiation as seen in the welds tested (Figure 6.5).

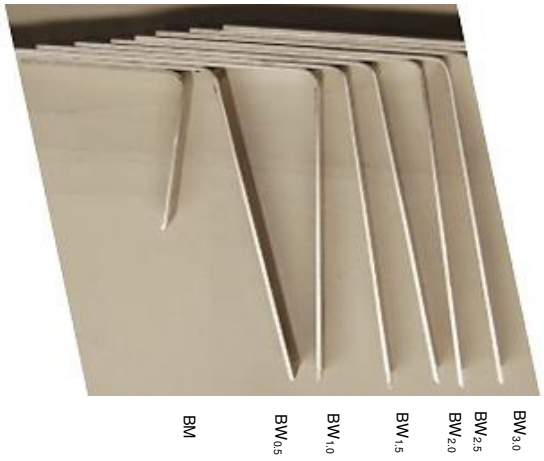

Figure 6.5- BT samples of the six BWs.

Tensile Test

To contribute to an industrial application, the analysis of mechanical performance is extremely important. Thus, the TT allowed to compare the welds' strength and deformation with the BM tested in the RD.

Figure 6.6 presents a graph with the average of the UTS of the six welds compared with the BM. This graph shows an increased UTS tendency from the $BW_{0.5}$ until $BW_{2.0}$, following to a patamar with similar values for $BW_{2.0}$, $BW_{2.5}$, and $BW_{3.0}$. The $BW_{2.0}$, $BW_{2.5}$, and $BW_{3.0}$ presented a very similar average UTS, with the $BW_{2.5}$ value a little larger than the $BW_{2.0}$. However, when considering the standard deviation, the $BW_{2.5}$ and $BW_{3.0}$ samples presented a larger variation than the $BW_{2.0}$ values. In this way, considering the UTS average associated with the deviation values, the $BW_{2.0}$ presented better and more constant mechanical performance when considered the UTS value, being around 90.8% of BM UTS.

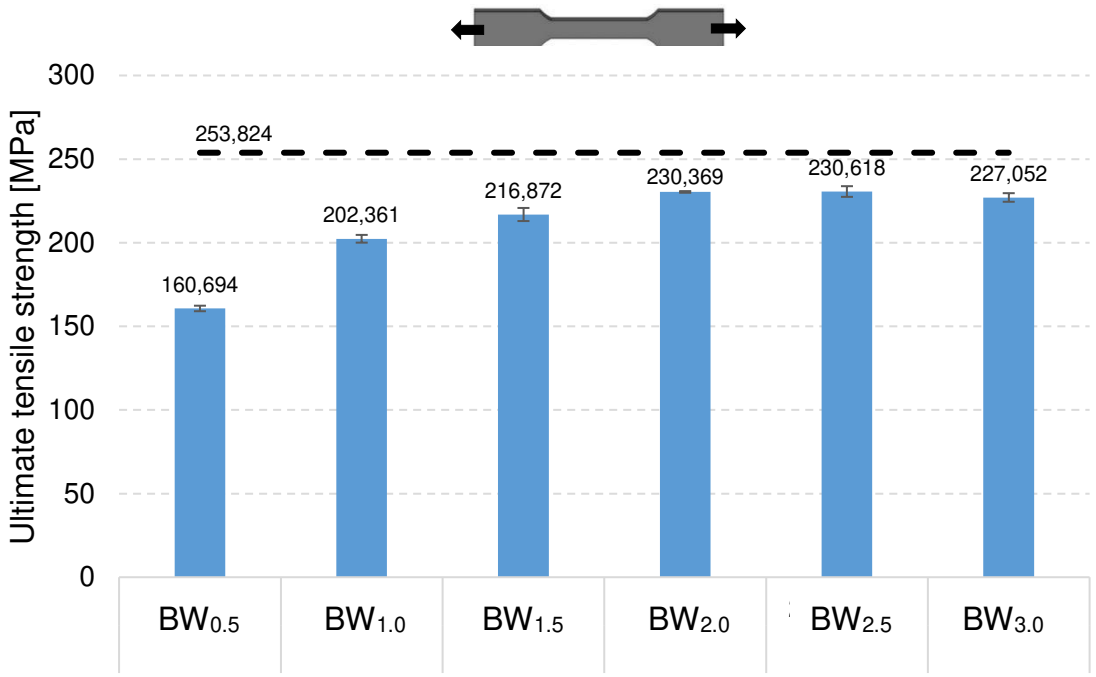

Figure 6.6 - UTS graph of the BW and BM in RD (dashed line).

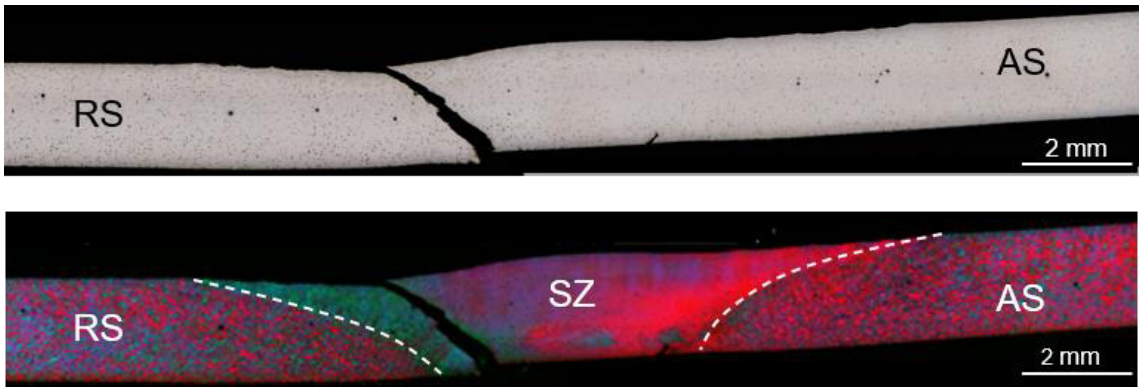

Figure 6.7 - Fracture model that occured in the six BW.

The welds tested presented a fracture model similar for all the welds, which happened in the SZ, as shown in Figure 6.7. This fracture behavior allows concluding that the tensile performance was mainly influenced by the change of the microstructure in SZ caused by the different tool traverse speeds. Thus, three main changes occur in the BM when the FSW is used, being in texture, grain structure, and grain size.

As exposed by Chowdhury et al. [30], the microstructure of the as-received AZ31 magnesium alloy rolled sheet consisted of some deformed and twinned

grains with Mn-Al inclusions, and with a strong crystallographic texture, with basal planes (0002) parallel to the sheet plane and $\langle 11\bar{2}0 \rangle$ direction aligned in the RD.

Thus, after the FSW, the combination of frictional heating, plastic deformation, and viscous dissipation cause DRX and basal planes relocation in the SZ, resulting in equiaxed and refined grains with the basal plane (0002) distributed around the pin surface [30].

In this way, the analyses of the weld's performance in the TT need to consider the sum of the texture, grain structure, and grain size contributions. Thereby, the lower UTS achieved in the $BW_{0.5}$ resulted from the lower tool traverse speed, which increased the heat input and the DRX; consequently, the recrystallized grain suffered growth, and the texture imposed by the friction was weak or more random due to the complete DRX.

Then, the increase of the UTS with the increase of the tool traverse speed is caused mainly due to the grain size refinement that is caused by the decrease of the heat input. Since the grain boundaries were the main obstacle to the dislocation slip, the joint with a smaller grain size would impose more restrictions to the dislocation movement and have a higher resistance to localized plastic deformation and, finally, present higher strength [30].

The patamar showed in Figure 6.6 by similar average UTS for $BW_{2.0}$, $BW_{2.5}$, and $BW_{3.0}$ may be caused by the lower expressive contribution of the grain refinement since, in this situation, the high tool traverse speed reduces the heat input, and the temperature reduction achieves a limit that can reduce the grain size. Thus, the grain achieves the size obtained by DRX in $BW_{2.0}$ and remains constant until $BW_{3.0}$.

However, when the FSW is used, both the stress and strain values decrease compared to the BM. The stress-strain curves in Figure 6.8 show a comparison of the $BW_{2.0}$ and BM curves. These curves show that although the joint efficiency (ratio of the UTS of the weld to the UTS of the BM) was high, around 90.8%, the elongation after FSW was relatively low compared to the BM, and thus, both the strength and ductility decreased.

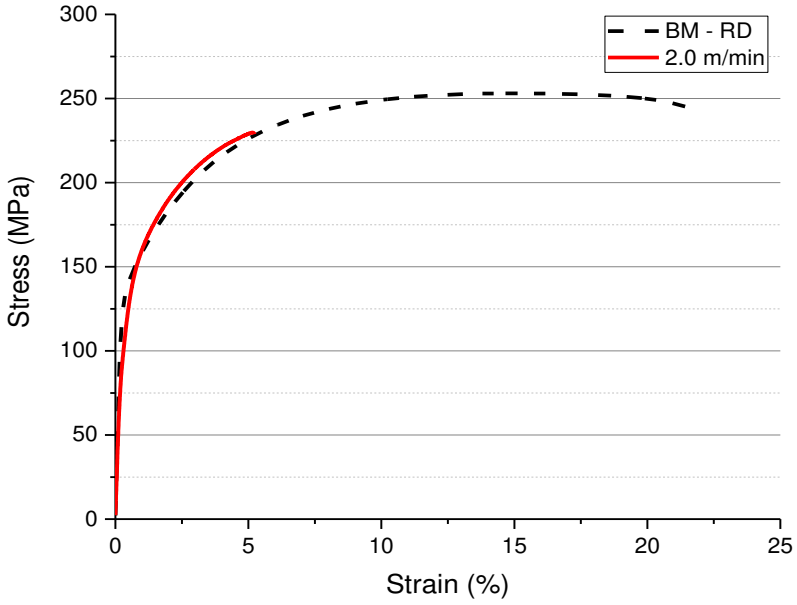

Figure 6.6- Stress versus strain curve of the $BW_{2.0}$ and BM-RD.

6.1.4 Hardness Test

The hardness analysis (Figure 6.9) shows three regions (SZ, TMAZ, and BM + HAZ) with different behaviors. Furthermore, the hardness profiles are determined by the trade-off between grain size and texture. The more refined grains resulted in greater hardness, and stronger texture resulted in greater softening.

In this regard, in SZ, the hardness was similar to the BM and constant from $BW_{1.0}$ to $BW_{2.5}$, being about 60 HV01. This constancy that is established with the increase in the tool traverse speed, is due to the continuous trade-off between the increase in grain refinement by the decrease of the heat input, and the increase in the {0001} <uwtv> β-fiber texture which, occurring together, balance the tendency of hardening and softening, respectively.

When analyzing the two-speed extremes, $BW_{0.5}$ and $BW_{3.0}$, the hardness profiles of the SZ were approximately parabolic, reaching a maximum value of approximately 60 HV_{01} and 70 HV_{01}, respectively. This parabolic behavior reflects

an imbalance between both factors, texture and grain size, due to a nullification/reduction of texture interference, resulting in a hardness profile driven mainly by the variation in grain size, which increases from the center to the end of the SZ.

In SZ, the texture is determined by the degree of friction, which increases with the lowest tool traverse speed, and by the degree of DRX, which increases with increasing temperature. Thus, in the $BW_{0.5}$, the lower tool traverse speed results in an increase in texture due to high friction of the material; however, the high temperatures developed caused an almost complete DRX making a weak and random texture, as reported by Chowdhury et al. [30].

In the $BW_{3.0}$, on the other hand, the higher tool traverse speed determines less friction, which resulted in a weaker texture, and the lower temperature developed results in DRX, even if in a less expressive way. Thus, in the $BW_{0.5}$, the combination of high DRX and friction leads to a nullification of the influence of the texture, and in the $BW_{3.0}$, the combination of reduced DRX and friction leads to less expressiveness of the texture in determining the hardness.

In $BW_{0.5}$ TMAZ, the decreasing of hardness approaching SZ is the result of the expressive softening caused by the strong texture due to high friction, and the less grain refinement resulted from the high heat input developed. Thereafter, there was a gradual decrease in texture and grain size, which resulted in higher hardness in the RS from $BW_{1.0}$ to $BW_{3.0}$. In AS, the reduced hardness values extended until $BW_{1.5}$, which shows the formation of stronger textures in AS compared to RS. From $BW_{2.0}$ to $BW_{3.0}$, the hardness was increased again in relation to SZ.

As for the BM + HAZ region, an approximately constant profile, around 60 HV_{01}, was verified in all samples due to a low distinction between the BM and HAZ microstructure, evidenced by the impossibility of determining the interface between both regions from the analysis of the hardness profile.

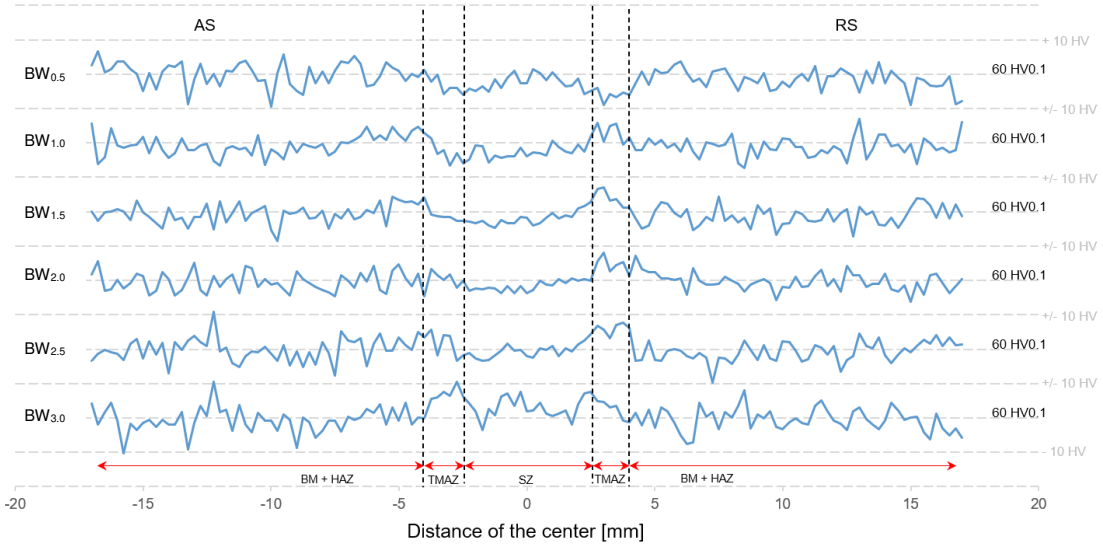

Figure 6.7- Hardness profile with three different regions: SZ, TMAZ, and HAZ+BM.

6.2 Overlap Joint Configuration

6.2.1 Macrostructural Characterization

In the same way as the BWs, the OWs had their superficial aspects analyzed as showed in Figure 6.10. The samples welded in both configurations A and B presented flashes when welded with the two lower tool traverse speeds: 1 m/min and 2 m/min (Figure 6.10 (A1), (A2), (B1), and (B2)). The use of the other two higher speeds, 3 m/min and 4 m/min, resulted in a good surface finishing without flashes and defects, as seen in Figure 6.10 (A3), (A4), (B3), and (B4).

In addition, the welds in a configuration B showed more flashes due to the higher plasticized material movement outside the shoulder to weld surface. The higher flash in OW_{B2} than in OW_{A2} allows supposing that the second configuration develops higher temperature, even when the same speed is used.

Figures 6.11 (A2) and (B3) show that the welds in configuration A started to present voids from the tool speed of 2 m/min and, on the other hand, in configuration B the voids start to be developed from the tool speed of 3 m/min. Considering the formation of voids as a consequence of the low temperature, which reduces the volume of plasticized material available to fill the weld region, it can then be concluded that configuration A showed a reduction in temperature at a lower tool traverse speed than configuration B. Thus, the temperature profile may not only be influenced by tool traverse speed but also by changing the weld configuration.

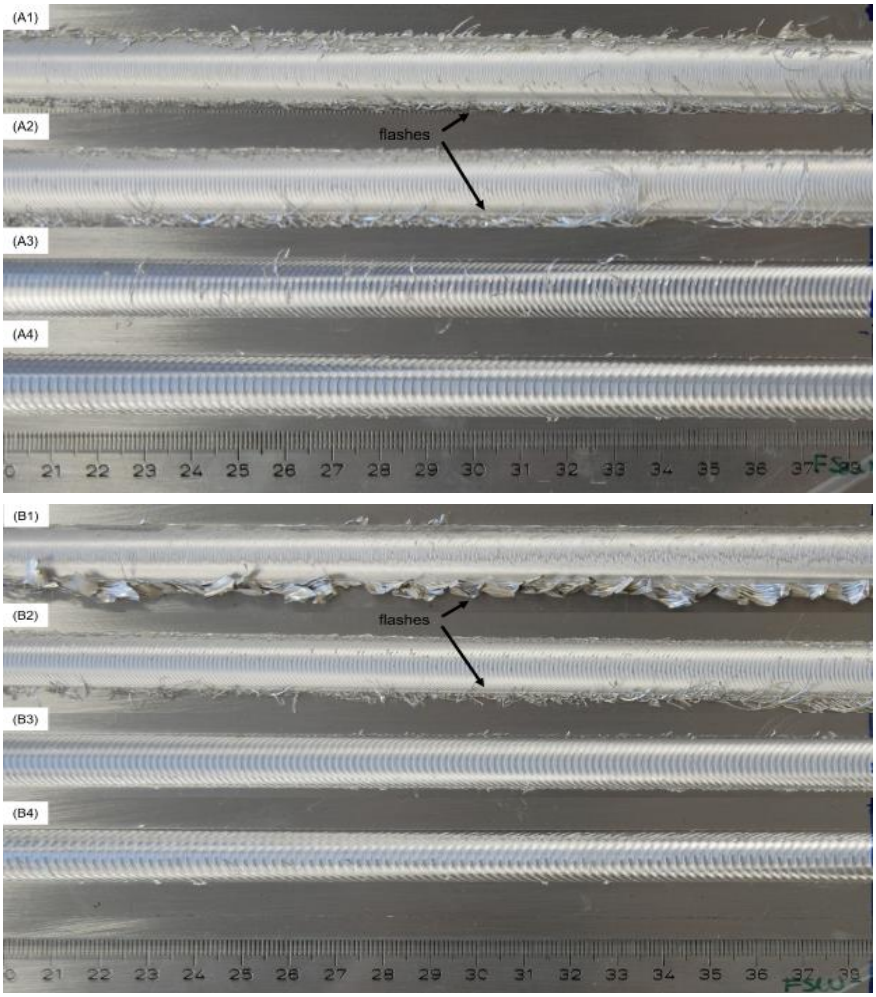

Figure 6.8- Superficial aspects of the OW_A and OW_B.

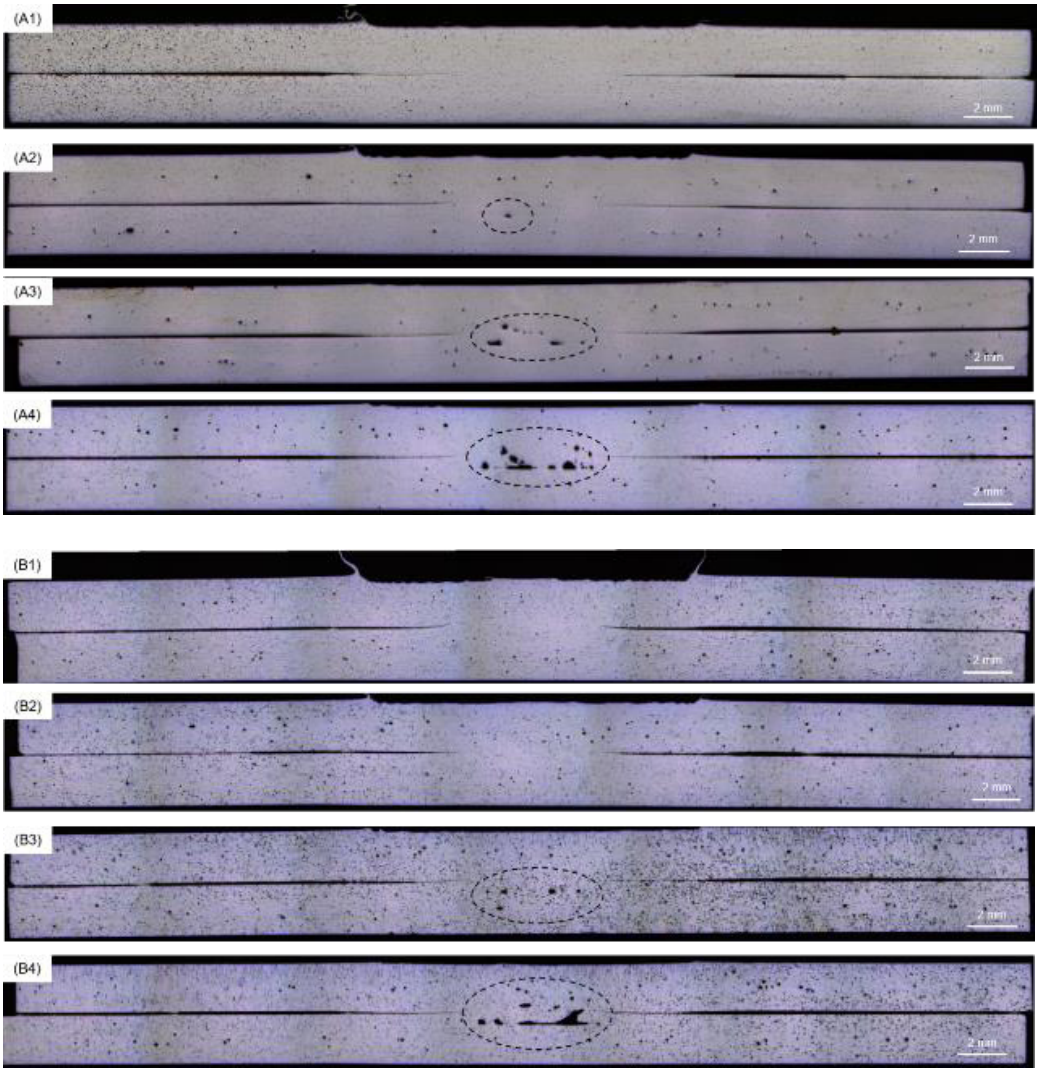

Figure 6.9- Cross section aspects of the OW_A and OW_B.

6.2.2 Microstructural Characterization

Similar to the BW exposed above, the welds developed by FSW in the overlap configuration also followed the typical pattern with three zones (SZ, TMAZ, and HAZ) as can be seen in Figure 6.12 (A), (B), (C) and (D). In addition, the microstructure of the weld, such as grain structure and twin formation, followed also the BW aspects as exposed in Figure 6.13.

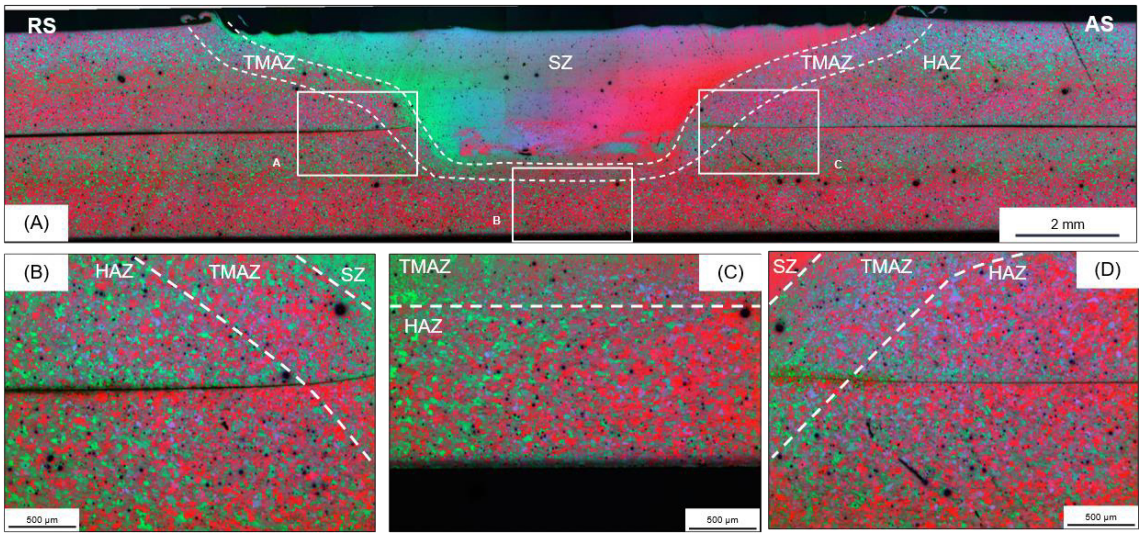

Figure 6.10- Three typical welds regions. In (A) the OW_{A2}, (B)SZ, TMAZ and HAZ on RS, (C) TMAZ and HAZ on weld root, and (D)SZ, TMAZ and HAZ on AS.

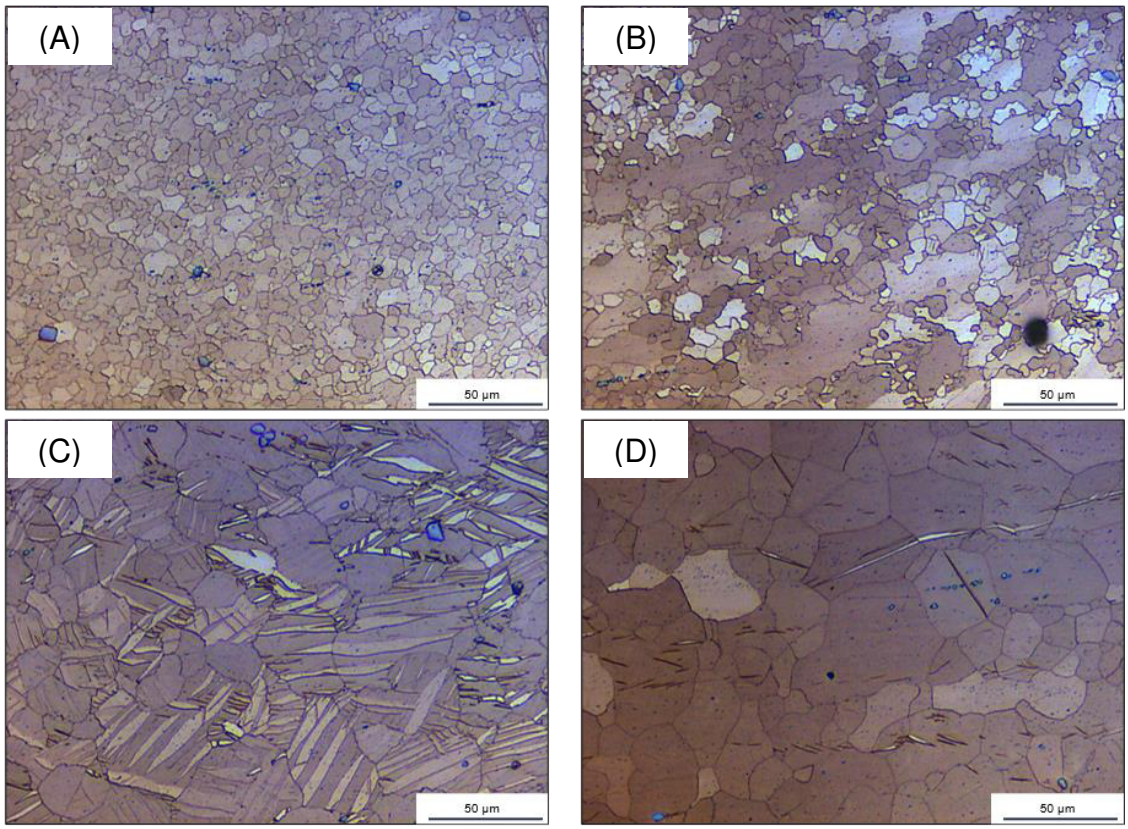

Figure 6.11- Weld microstructures in (A) SZ, (B) TMAZ, (C) HAZ and (D) BM.

The peculiarities of this weld design were the presence of plates junction parallel to the weld line forming two typical discontinuities as shown in Figure 6.14. On the AS, the hooking feature (Figure 6.14 (A)) was formed due to the downward motion of the material that is in front of the tool and after it is deposited in the wake of the pin. However, on the RS was formed the cold lap feature (Figure 6.14 (B)), which is resulted from a complex set of material movements. The hooking on the AS and the cold lap feature on the RS were similarly found in another study by Yuan et al. [9], and this structured pattern was equal for all the samples welded by the overlap in this work..

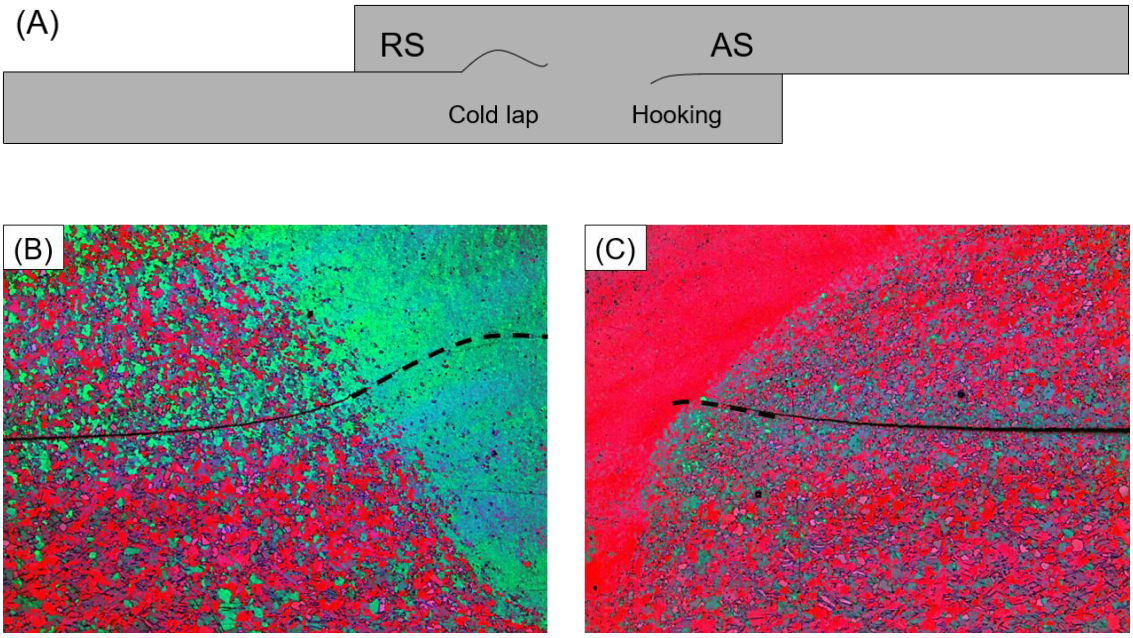

Figure 6.12- (A) Model of the two discontinuities formed in the OW. In (A) the cold lap on RS, and (B) the hooking on AS.

6.2.3 Lap Shear Test

To analyze the mechanical performance of these welds, the samples were tested by LST. Based on the results, two distinct comparatives can be established, being one between the welds with different configurations (A and B) and the other between the welds with the same configuration (A or B).

Comparing the lap shear results of configuration A with configuration B, the graph in Figure 6.15 allowed us to confirm a superior expressive performance of the samples welded in configuration B. Comparing the best values of each configuration, the OW_{B3} shear stress was about 71% higher than OW_{A2}.

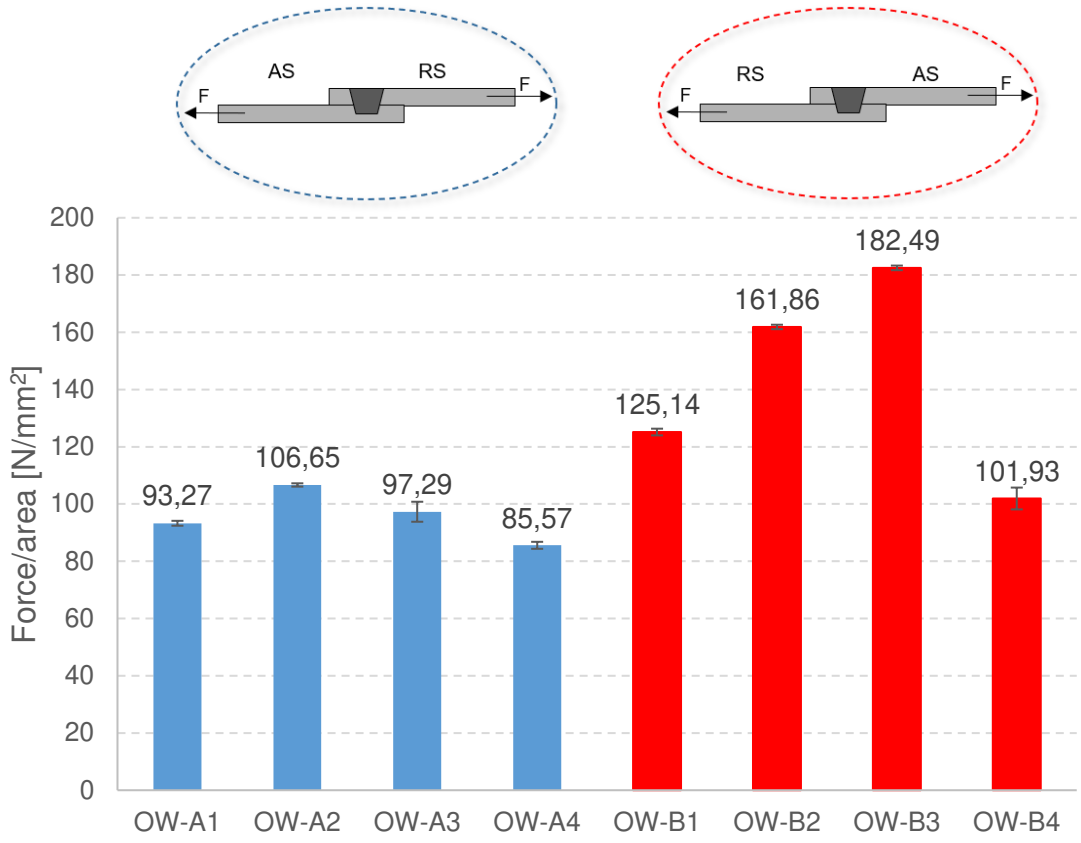

Figure 6.13- Graph of the lap shear performance of the OW_A and OW_B.

First of all, most of the welds fractured in the top sheet on the loading side due to the higher tension developed in this region, as shown in Figure 6.16 that presents the load configurations and the force lines for each configuration. Therefore, the configuration A welds fractured on the RS, and the configuration B welds fractured on the AS, as shown in Figure 6.16 (A) and (C). The exception was the OW_{A4}, which due to the high concentration of voids, had a longitudinal propagation of the fracture resulting in the detachment of the plates in the SZ (Figure 6.16 (E)).

Then, what determined the fracture stress, in addition to the concentration of the voids, was the hooking or the cold lap presence in the loading side, since

each of these discontinuities provides a different EST. The EST is lower where the cold lap is formed, thus as the cold lap is developed in the RS and the configuration A welds were loaded on the RS, these samples had lower EST tested and, consequently, lower fracture stress when compared with the configuration B samples.

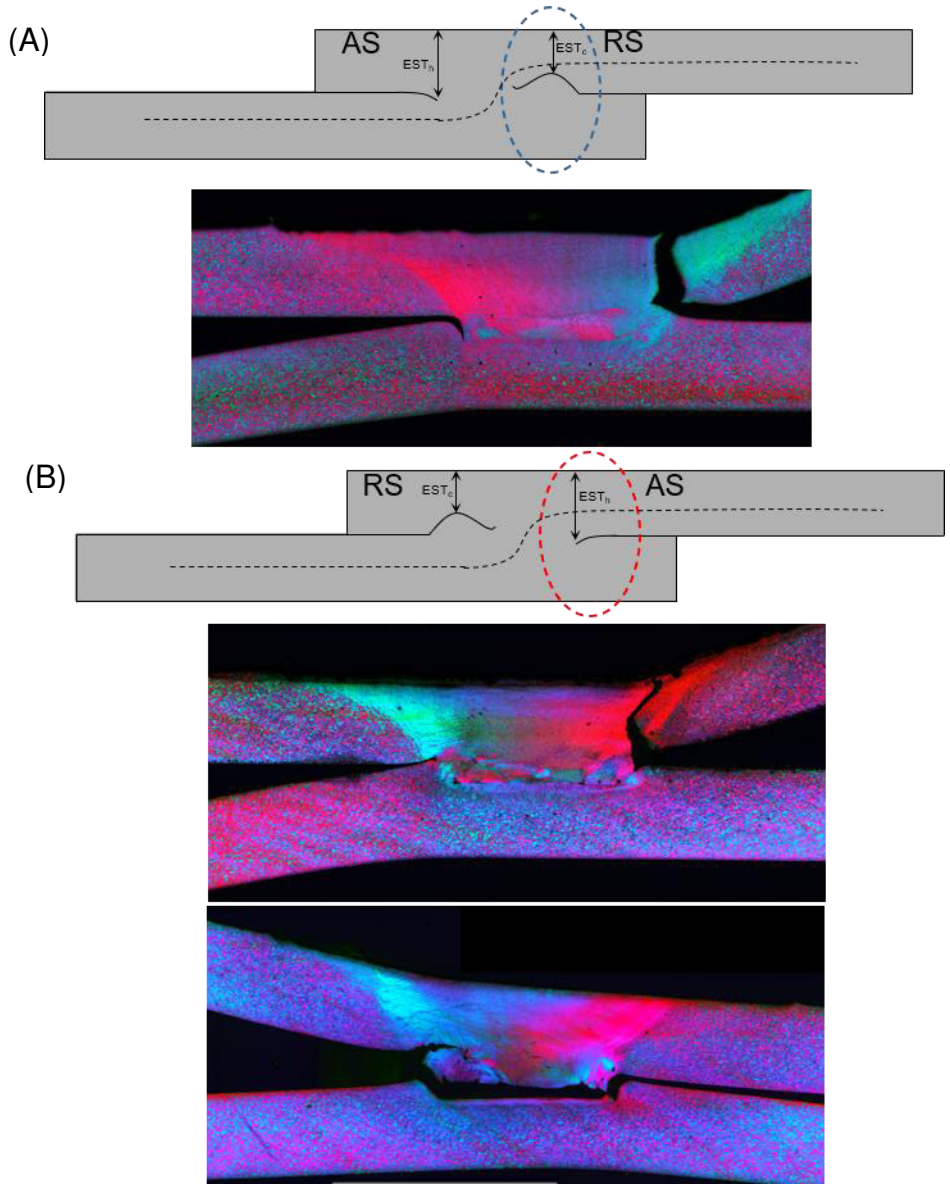

Figure 6.14- Fracture model in (A) OW_A and (B) OW_B.

Comparing the lap shear results of configuration A (Figure 6.17), it is observed that the BW_{A2} had the best performance with 106.65 N/mm^2. Considering that these four welds fractured as exposed above, from the cold lap in the SZ on the RS, the improvement from OW_{A1} to OW_{A2} resulted from the grain refinement due to the increased speed (Figure 6.19), which introduced more grain contours and difficulted fracture propagation. However, the decreasing strength from OW_{A2} to OW_{A4} is caused by more voids introduced in the SZ when the tool traverse speed is higher than 2 m/min, such as 3 m/min and 4 m/min (Figure 6.17). The voids act as a stress concentrator and a shortcut for the crack to spread through the cold lap. Thus, when in high concentrations, the voids start cracking at low tensions, and this crack grows more easily through this shortcut, propagating until the fracture.

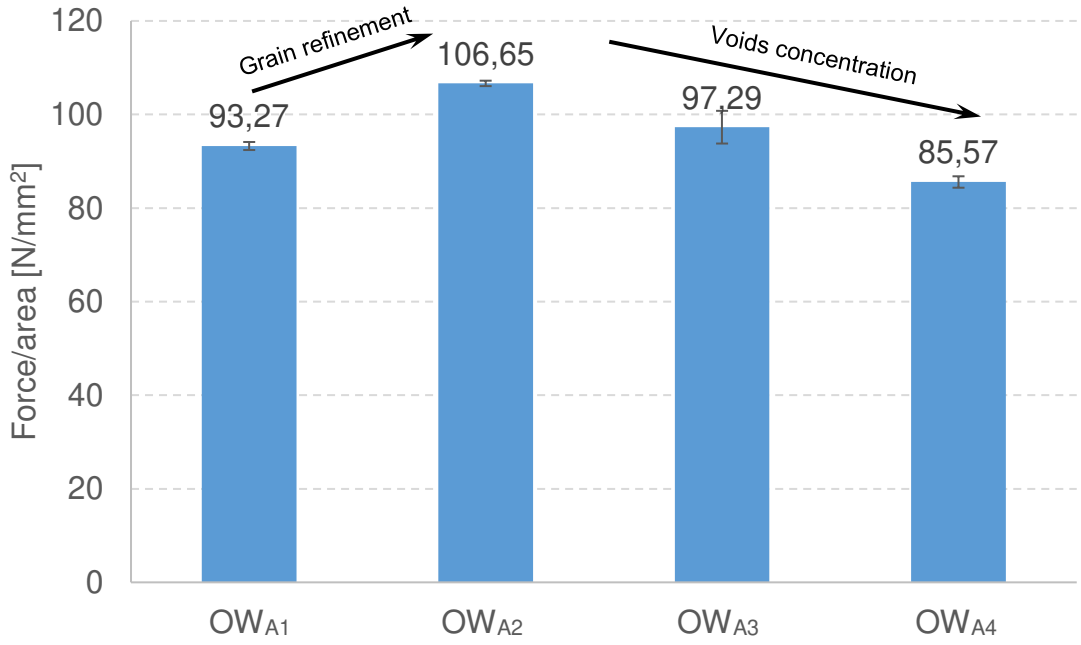

Figure 6.15- Lap shear graph of the OW_A.

The lap shear results of configuration B welds presented similar behavior of configuration A. The fracture of these samples occurred from the hooking in the SZ on the AS, being similar for the OW_{B1}, OW_{B2}, and OW_{B3}. However, the OW_{B4} presented fracture by the detachment of the plates. Figure 6.18 shows an increase in strength from OW_{B1} to OW_{B3} followed by a decrease from OW_{B3} to

OW_{B4}. The increase in strength by increasing tool traverse speed was caused by the grain refinement, as exposed above (Figure 6.19). On the other hand, the strength decrease to OW_{B4} was caused by the high voids concentration, which started longitudinal crack propagation with fracture by the detachment of the plates in the SZ (Figure 6.16 (B)).

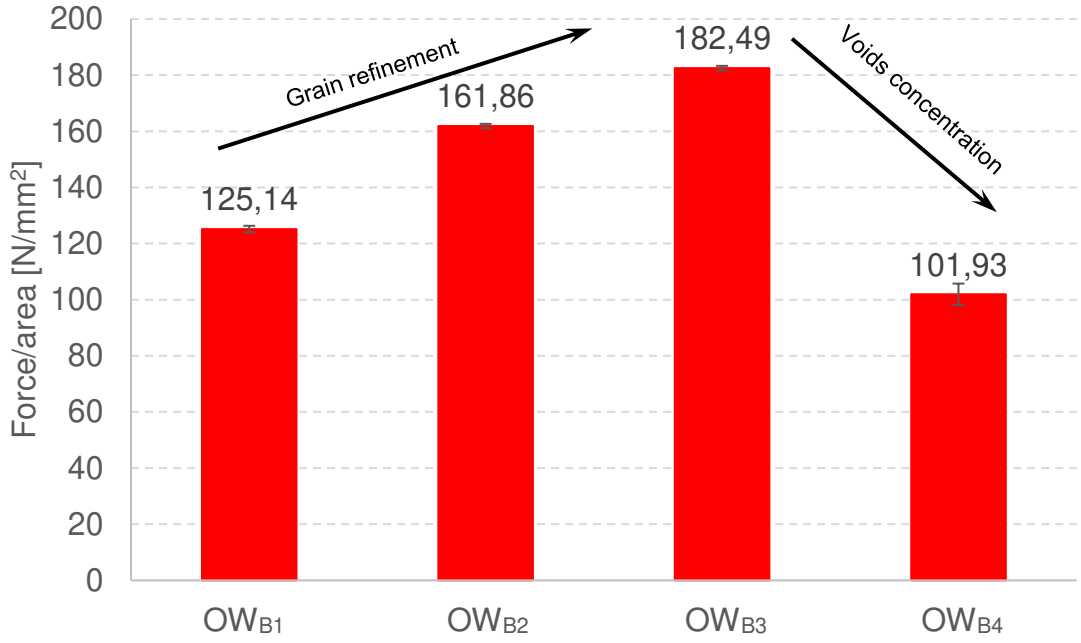

Figure 6.16- Lap shear graph of the OW_B.

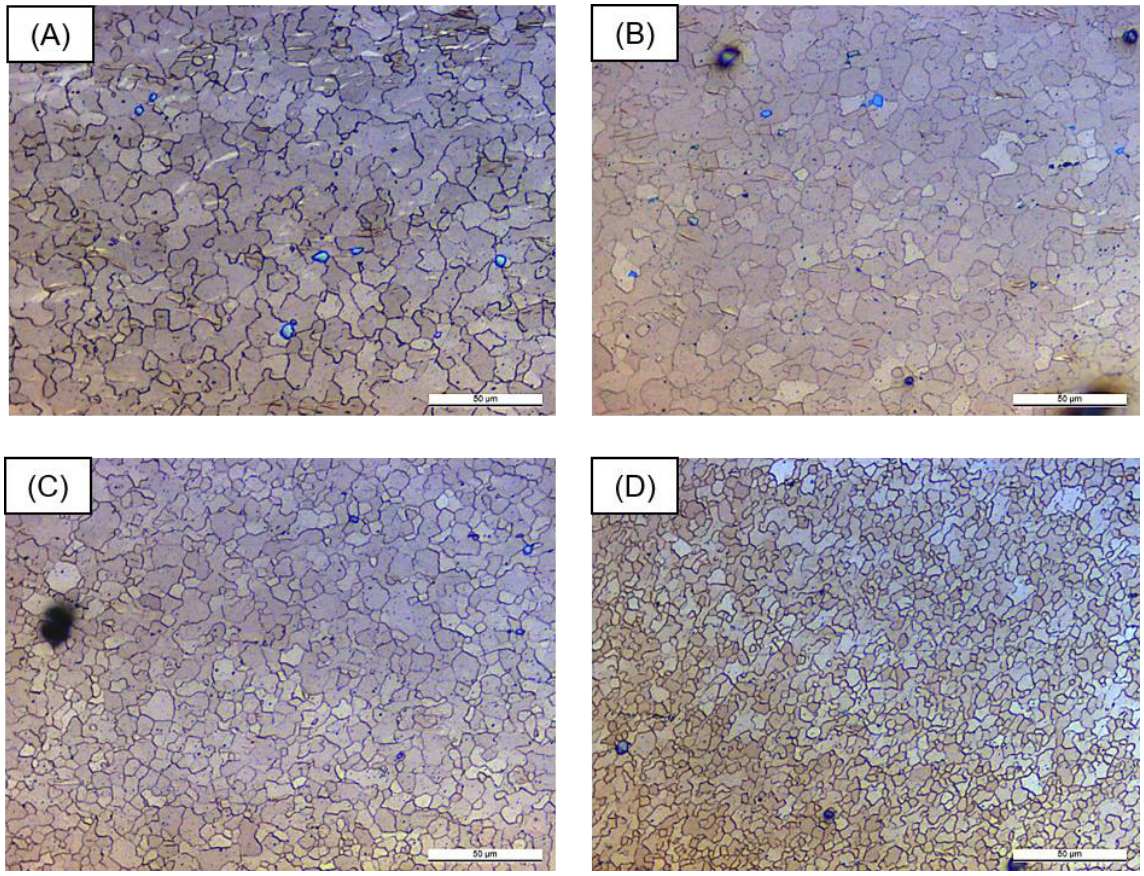

Figure 6.17- Grain refinement in the OW_B using (A) 1m/min, (B) 2 m/min, (C) 3 m/min, and (D) 4 m/min.

6.2.4 Hardness Test

The The analysis of the hardness profiles of the eight welds made it possible to distinguish three regions with different hardness behaviors, namely SZ, TMAZ, and BM + HAZ. As well as discussed for the BW samples, the hardness profiles were determined by a trade-off between grain size and texture.

The configuration A samples showed, on average, slightly higher hardness values than the configuration B samples. The SZ of these samples showed constant hardness profiles with a hardness similar to the BM: 60 HV_{01}. A distinction between these four samples was that the samples OW_{A1} and OW_{A2} presented hardness values close to 55 HV_{01} and the samples OW_{A3} and OW_{A4} showed hardness values close to 60 HV_{01}. Thus, it can be inferred that the constant hardness profile of these regions is due to the balance between texture

and grain size, and the higher hardness for OW_{A3} and OW_{A4} welds is due to the increased tool traverse speed, which increases grain refinement.

For TMAZ, the hardness profile of this region is mostly determined by the degree of texture established during the welding process. Thus, by analyzing the curves in Figure 6.20, it was found that the behavior, as well as the hardness values of this region, little changed from one weld to another. Thus, it is possible to estimate that there is little distinction in the degree of texture in the TMAZ of these four welds.

The analysis of the hardness profiles of configuration B samples shows that the SZ of samples OW_{B1}, OW_{B2}, and OW_{B3} exhibits a constant hardness of approximately 55 HV_{01}. The OW_{B4} sample, on the other hand, although presented a similar constancy profile, the values were around 60 HV_{01}. This constant hardness profile also suggests a balance between texture and grain refinement.

For TMAZ, on RS, the hardness values showed an increase from OW_{B1} to OW_{B4} due to the reduction of the tool traverse speed, which in turn reduced friction and texture formation; therefore, there was a reduction in the softening due to this weakening of the texture. On the AS, the hardness values of the samples OW_{B1}, OW_{B2}, and OW_{B3} were similar and at an average of 55 HV_{01}, suggesting little variation in texture between the samples. However, there was an increase in hardness for OW_{B4}, which was close to 65 HV_{01}.

Finally, the BM + HAZ regions of the eight welds showed similar hardness profile and difficult to distinguish between HAZ and BM, as occurred in the BW samples.

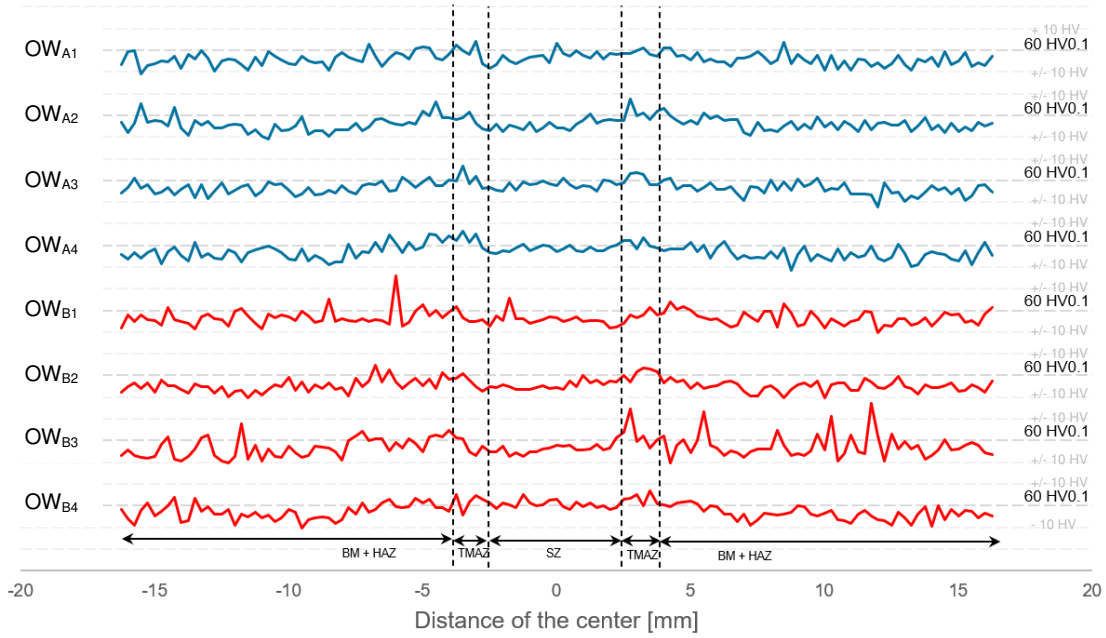

Figure 6.18- Hardness profiles of the OW_A and OW_B welds.

7 CONCLUSIONS

AZ31 magnesium alloy plates with 2 mm thickness were welded by FSW in BW and OW configurations. For the BW, six welds were prepared, $BW_{0.5}$ to $BW_{3.0}$, with an increased tool traverse speed varied from 0.5 to 3 m/min. For the OW, eight welds were made, four with configuration A (AS in joint line, OW_{A1} to OW_{A4}), and four with configuration B (RS in joint line¸ OW_{B1} to OW_{B4}), with an increased tool traverse speed varied from 2 to 5 m/min.

The characterization of BW allowed the following findings:

- Superficially, the BWs showed a good surface finishing, except for the $BW_{0.5}$, which presented flashes due the higher temperature developed by lower tool traverse speed favoring the get out of plasticized material to the shoulder side;
- In the cross-section, the samples did not show macroscopic defects, only flashes in $BW_{0.5}$ and reduced thickness in $BW_{0.5}$, $BW_{1.0}$, and $BW_{1.5}$;
- The micrographs allowed to verify the three typical regions resulting of the FSW, SZ, TMAZ, and HAZ, as well as the two main interfaces, SZ/TMAZ and TMAZ/HAZ;
- The analysis of the weld root by the BT did not show the beginning of fracture at the root, which ruled out the presence of lack of fill or voids as stress concentrators;
- The UTS increased with the increase of tool transverse speed from $BW_{0.5}$ to $BW_{2.0}$ and reached a plateau from $BW_{2.0}$ to $BW_{3.0}$. The $BW_{2.0}$ sample had the best performance when considered together UTS average and deviation values with a UTS of 90.8% of BM;
- The analysis of the stress *versus* strain curve found high UTS values, but a significant reduction in strain;
- The fracture of the samples occurred in the SZ on the RS side, being, therefore, the microstructure of the SZ the main responsible for the weld's performance in the TT;
- The SZ hardness was similar to the HAZ and BM, with values around 60 HV_{01} due to a trade-off between grain size and texture. The TMAZ

presented higher hardness values than SZ on RS of the $BW_{1.0}$, and on AS of the $BW_{2.0}$.

The main findings after the characterizations of the OW were:

- OW_{A1}, OW_{A2}, OW_{B1}, and OW_{B2} showed flashes, and OW_{A3}, OW_{A4}, OW_{B3}, and OW_{B4} showed good surface finish;
- In the cross-section, the samples OW_{A1}, OW_{B1}, and OW_{B2} did not present macroscopic defects, while the others presented voids in the SZ;
- The micrographs allowed to verify similarities between the SZ, TMAZ, and HAZ of the eight welds and, also, the presence of discontinuities such as cold lap and hooking, on RS and AS, respectively;
- The welds performance in the LST showed higher values for samples with configuration B than with configuration A due to the greater EST presented in AS, where fractures occur for OW_{B1}, OW_{B2}, and OW_{B3}. When comparing samples of the same configuration, the increased shear strength is mainly due to the grain refinement of SZ, whereas the decreased strength is mainly due to the increase in void concentration;
- The SZ hardness of the eight welds was similar to the hardness values of HAZ and BM, being around 60 HV_{01}, whereas TMAZ presented values higher than those of SZ due to the grain refinement by DRX and the lower softening due to the weak local texture.

From these results, it can be inferred some general conclusions that the tool traverse speed has a strong correlation with the weld temperature; interfering in the material flow, grain size, and texture, and, consequently, determining the tensile strength, shear strength, and hardness.

However, some specific conclusions about the influence of the tool traverse speed could be verified, keeping constant the welding process (FSW), the alloy (AZ31), the plate thickness (2 mm), the tool parameters and the tool rotation speed (2000 rpm). The BW specific conclusions were:

- Macroscopic defects in the cross-section are avoided using tool traverse speeds of 0.5 until 3.0 m/min;

- Good surface finish is achieved with values of 1.0 until 3.0 m/min;
- High and constant UTS is achieved using 2.0 m/min;

The OW specific conclusions were:

- Macroscopic defects are avoided using tool traverse speed of 1.0 m/min in configuration A, and values of 1.0 until 2.0 m/min in configuration B;
- Good surface finish is achieved using values of 3.0 until 4.0 m/min;
- High shear stress is achieved using 3.0 m/min in configuration B.

8 FUTURE WORKS

Since automotive seats are a complex component, many welds designs could be required. Then, in addition to butt and overlap welding, other FSW weld designs can be studied. Still, based on the complexity of the seats, plates with different thicknesses may be necessary to enable the required material replacement.

Because of the wide range of parameters involved in the FSW, parameters control is an important way to achieve the mechanical properties required. Then, the study of the tool rotation speed and axial force interference can contribute to obtaining better mechanical performance for the welds. Also, the FSW properties are directly affected by the tool used in the process. In this way, the study of the tool design and dimensions variability can contribute to better control and optimization of the material replacement by FSW.

Therefore, in addition to the analysis of the tool traverse speed in the FSW of 2 mm thick AZ31 plates in butt and overlap configurations; the exploration of new designs, applied to other plate thicknesses, varying the welding parameters, as well as the tool, will contribute to a better and more effective service to the industrial demand for reducing the weight of the car seats.

9 REFERENCES

[1] KIANI, M. et al. Design of lightweight magnesium car body structure under crash and vibration constraints. *Journal of Magnesium and Alloys*, v.2, p.99-108, 2014.

[2] WILBERFORCE, T. et al. Developments of electric cars and fuel cell hydrogen electric cars. *International Journal of Hydrogen Energy*, v.42, p.25695-25734, 2017.

[3] LUO, A. A.; SACHDEV, A.K. Applications of magnesium alloys in automotive engineering. *In: BETTLES, C.; BARNETT, M.* Advances in wrought magnesium alloys: Fundamentals of processing, properties and applications. *Woodhead Publishing,* p.393-426, 2012.

[4] WEN, T. et al. Influence of high frequency vibration on microstructure and mechanical properties of TIG welding joints of AZ31 magnesium alloy. *Transactions of Nonferrous Metals Society of China,* v.25, p.397-404, 2015.

[5] KISHORE, N. B. et al. Characterization of microstructure and deformation behaviour of resistance spot welded AZ31 magnesium alloy. *Material Science and Engineering: A,* v.549, p.149-156, 2012.

[6] MISHRA, R. S.; MA, Z. Y. Friction stir welding and processing. *Materials Science and Engineering R*, v.50, p.1-78, 2005.

[7] COMMIN, L. et al. Friction stir welding of AZ31 magnesium alloy rolled sheets: Influence of processing parameters. *Acta Materialia*, v.57, p.326-334, 2009.

[8] YANG, Q. et al. Effect of tool geometry and process condition on static strength of a magnesium friction stir lap linear weld. *Materials Science and Engineering A*, v.528, p.2463-2478, 2011.

[9] YUAN, W. et al. Study of top sheet thinning during friction stir lap welding of AZ31 magnesium alloy. *Science and Technology of Welding and Joining*, v.17, p.375-380, 2012.

[10] MORAES, J. F. C. et al. Effect of overlap orientation on fatigue behavior in friction stir linear welds of magnesium alloy sheets. *International Journal of Fatigue*, v.100, p.1-11, 2017.

[11] UGENDER, S. Influence of tool pin profile and rotational speed on the formation of friction stir welding zone in AZ31 magnesium alloy. *Journal of Magnesium and Alloys*, v.6, p.205-213, 2018.

[12] ELMOGAHZY, Y. E. Engineering textiles: Development of textile fiber products for transportation applications. *Woodhead Publishing*, ed.2, c.14, p.435-474, 2009.

[13] Special report: vehicle lightweighting. Automotive World. Available: < https://www.a3ps.at/blog/special-report-vehicle-lightweighting>. Accessed: 07 Dec. 2019.

[14] POWELL, B.; KRAJEWSKI, P.; LUO, A. Magnesium alloys for lightweight powetrains and automotive structures. *Materials, Design and Manufacturing for Lightweight Vehicles*, c.4, p.125-186, 2021.

[15] LIU, L. Welding and Joining of Magnesium Alloys: Welding metallurgy of magnesium alloys. *Woodhead Publishing*, c.2, p.9-15, 2010.

[16] POLMEAR, I. et al. Magnesium alloys. Light Alloys: metallurgy of the light metals. *Butterworth-Heinemann,* ed.5, c.6, p.287-367, 2017.

[17] QUAN, Y. et al. Effects of heat input on microstructure and tensile properties of laser welded magnesium alloy AZ31. *Materials Characterization*, v.59, p.1491-1497, 2008.

[18] HUTSCH, L. L. et al. Increased room temperature formability of Mg AZ31 by high speed friction stir processing. *Materials and Design*, v.54, p.980-988, 2014.

[19] FORCELLESE, A. et al. Formability and Microstructure of AZ31 Magnesium Alloy Sheets. *Key Engineering Materials*, v.344, p.31-38, 2007.

[20] CALLISTER, W. D. Materials Science and Engineering: An Introduction. *Wiley,* ed.8, 2009.

[21] PRADEEP, A. A Review on Friction Stir Welding of Steel. *International Journal of Engineering Research and Development,* v.3, p.75-91, 2012.

[22] THOMAS, W. M. et al. Feasibility of friction stir welding steel. *Science and Technology of Welding and Joining*, v.4, p.365-372, 2013.

[23] PADMANABAN, G.; BALASUBRAMANIAN, V. Selection of FSW tool pin profile, shoulder diameter and material for joining AZ31B magnesium alloy – An experimental approach. *Materials and Design*, v.30, p.2647-2656, 2009.

[24] SCIALPI, A.; FILIPPIS, L. A. C.; CAVALIERE, P. Influence of shoulder geometry on microstructure and mechanical properties of friction stir welded 6082 aluminium alloy. *Materials and Design*, v.28, p.1124-1129, 2007.

[25] ROWE, C. E. D. et al. Advances in tooling material for friction stir welding. Available:<https://www.yumpu.com/en/document/read/23423271/advances-in-tooling-materials-for-friction-stir-welding-innoval->. Accessed: 18 Jan. 2021.

[26] SUHUDDIN, U. F. H. R. et al. Grain structure evolution during friction-stir welding of AZ31 magnesium alloy. *Acta Materialia*, v.57, p.5406-5418, 2009.

[27] ALBANNAI, A. Review the common defects in friction stir welding. *International Journal of Scientific e Technology Research*, v.9, p.318-329, 2020.

[28] HASAN, A. CFD modelling of friction stir welding (FSW) process of AZ31 magnesium alloy using volume of fluid method. *Journal of Materials Research and Technology,* v.8, p.1819-1827, 2019.

[29] MIRONOV, S. et al. Microstructure evolution during friction-stir welding of AZ31 magnesium alloy. *Acta Materialia*, v.100, p.301-312, 2015.

[30] CHOWDHURY, S. et al. Friction stir welded AZ31 magnesium alloy: microstructure, texture, and tensile properties. *Metallurgical and Materials*

Transactions A: Physical Metallurgy and Materials Science, v.44, p.323-336, 2013.

[31] XUNHONG, W.; KUAISHE, W. Microstructure and properties of friction stir butt-welded AZ31 magnesium alloy. *Materials Science and Engineering A*, v.431, p.114-117, 2006.

[32] ÇAM, G.; MISTIKOGLU, S. Recent developments in friction stir welding of Al-alloys. *Journal of Materials Engineering and Performance*, v.23, p.1936-1953, 2014.

[33] THREADGILL, P. L. Terminology in friction stir welding. *Science and Technology of Welding and Joining*, v.12, p.357-360, 2013.

[34] PAN, W. et al. A new smoothed particle hydrodynamics non-Newtonian model for friction stir welding: process modeling and simulation of microstructure evolution in a magnesium alloy. *International Journal of Plasticity*, v.48, p.189-204, 2013.

[35] KIM, M. S. et al. Simulation of microtexture developments in the stir zone of friction stir-welded AZ31 Mg alloys. *International Journal of Plasticity*, v.94, p.24-43, 2017.

[36] XIN, R. et al. Influence of welding parameter on texture distribution and plastic deformation behavior of as-rolled AZ31 Mg alloys. *Journal of Alloys and Compounds*, v.670, p.64-71, 2016.

[37] GULATI, P.; SHUKLA, D. K.; GUPTA, A. Defect formation analysis of Friction Stir welded Magnesium AZ31B alloy. *Materials Today: Proceedings*, v.4, p.1005-1012, 2017.

[38] LIU, D. et al. Effect of textural variation and twinning activity on fracture behavior of friction stir welding AZ31 Mg alloy in bending tests. *Jornal of Alloys and Compounds*, v.693, p.808-815, 2016.